Doctoral Thesis

博士学位論文

Development of the Total Energy Calculation Program within the Self-consistent GWΓ Approach Based on the All-electron Mixed Basis Approach

全電子混合基底法に基づく自己無撞着 GWΓ 法による全エネルギー計算プログラムの開発

Department of Physics, Graduate School of Engineering,
Yokohama National University
横浜国立大学大学院 工学府

Riichi Kuwahara
桑原 理一

September 2014

平成 26 年 9 月

Contents

Chapter 1 Introduction 1

Chapter 2 GW Approximation with the All-Electron Mixed Basis Approach: Validity of Virial Theorem 5
2.1 Introduction 5
2.2 Theory 7
2.3 Methodology 14
2.4 Results and Discussion 15

Chapter 3 Linearized GW Approach Satisfying the Ward Identity: Total Energy Calculation Based on the Luttinger–Ward Functional 27
3.1 Introduction 27
3.2 Theory 29
3.3 Methodology 37
3.4 Results and Discussion 38

Chapter 4 GWΓ with the All-Electron Mixed Basis Approach 43
4.1 Introduction 43
4.2 Theory 43
4.3 Methodology 54
4.4 Results and Discussion 55

Chapter 5 Summary 59

References 63

Chapter 1

Introduction

A first-principles calculation method is becoming a standard tool to predict various materials properties. There are some different approaches based on first-principles. Among them, the density functional theory (DFT) [1] as well as Hartree–Fock theory is widely prevalent and a firm position has been established in the world of quantum physics and chemistry [2].

The total energy is the most important property of materials in order to discuss a stability of different conformation of molecules and polymorph of crystals, and the DFT has achieved a great success in this point of view. However, the DFT is valid only for the ground state, thus it cannot be used to predict the band gap and optical properties of materials correctly.

Under these circumstances, a method that can be applicable to the calculations of excited states is highly desired. The GW method proposed by Hedin [3] is one of such methods, which is based on the Green's function method in the many-body perturbation theory. Within this Green's function method, the concept of a quasiparticle is introduced as an apparent particle without an interaction each other but dressed by an effective interaction. The virtual cloud surrounding the quasiparticle is represented with the self-energy $\Sigma[G]$ in Green's function G. In the GW method, the effective interaction is given by the dynamically screened Coulomb interaction W composed of the polarization function P within the random phase approximation (RPA). This self-consistent GW approach (SCGW) gives quasiparticles wave functions and energies as a self-consistent solution of Dyson's equation. The important point of this approach can be regarded as the conserving approximation proposed by Baym and Kadanoff [4], and as a consequence, the conservation laws of the number of particles, momentum, and angular momentum is satisfied. In addition, the virial theorem

stating that minus of the total potential energy divided by the total kinetic energy is exactly equal to 2 in any systems interacting only with the Coulomb interaction is also satisfied within the conserving approximation [5], although there has been no explicit report confirming it numerically.

So far, the so-called 1-shot GW approximation (1-shot GW) has been successfully applied to the prediction of the band gap of crystals and the energy gap of clusters and molecules [6–9]. However, 1-shot GW is a non self-consistent method, i.e., Dyson's equation is not solved self-consistently. Thus, quasiparticle wave functions are not updated, and virial theorem is not satisfied. On the other hand, in the SCGW, as a well known shortcoming, the band gap and energy gap is overestimated compared to the 1-shot GW [10]. One reason of this overestimation the Ward–Takahashi identity (WTI) [11] is not satisfied within the SCGW framework. In order to satisfy the WTI, the vertex correction must be taken into account to the polarization function and the self-energy, and this method is called the GWΓ method. This is a very challenging work due to the complexity of the vertex function, and solving the vertex function as a self-consistent solution of the Bethe-Salpeter equation requires a huge computational load. As efforts to improve the SCGW method, there have been some studies to take account of the local field correction with the exchange-correlation kernel f_{xc} [12,13] in the framework of the many-body perturbation theory. The correction is explicitly included only in the polarization function, and the implicit vertex correction beyond the RPA should be included in the dynamically screened interaction. In the sense of the WTI, however, the vertex correction should be explicitly introduced not only the polarization function but also the self-energy. Thus this approach does not satisfy the WTI. Moreover, there is arbitrariness for choosing f_{xc}, and it needs to be determined from other frameworks, e.g., the time-dependent density functional theory.

For the calculation of the total energy within the GW approximation, Luttinger and Ward [14] first showed that the total energy is given by the Luttinger–Ward (LW) functional $\Phi[G]$ and some other contributions easily estimated, and the self-energy $\Sigma[G]$ is derived from a functional derivative of $\Phi[G]$ with respect to Green's function G. The important point is that it satisfies the variational principle. Using this fact, the total energy has been estimated by a robust calculation of the LW functional Φ from the one-shot GW and other approaches [5, 15, 16].

Another difficulty in the quasiparticle representation is that the quasiparticle wave functions are non-orthonormal and linearly dependent due to the energy dependence

of the self-energy. One way to solve this problem is to use Löwdin's symmetrized orthonormalization procedure, but there is a big question how to deal with this energy dependence when the quasi-particle equation is solved self-consistently.

In this study, I implement the self-consistent GW approaches to our all-electron mixed basis code, TOMBO. In our mixed basis code, one-particle wave functions are expanded with atomic orbitals (AO) and plane waves (PW). This approach can describe any electronic states such as deep core states and plane wave like states above the vacuum level. The first purpose of this thesis is, therefore, to confirm the validity of virial theorem in the GW calculation. In order to resolve the problem of the energy dependence in the self-energy, I propose a linearized self-consistent GW approach (LGW). The LGW is an improved approach for the GW and I found that the Ward identity (Ward–Takahashi identity in the $\boldsymbol{q} = 0$ and $\omega - \omega' = 0$) is satisfied in the LGW. The second purpose of this thesis is, therefore, to develop this LGW approach and demonstrate its ability. The third purpose of this thesis is to include the first-order vertex correction of the electron-electron Coulomb interaction in the self-consistent GW and LGW approaches.

This thesis is composed of five chapters. In the second chapter, I will give the detailed description of the GW theory and the algorism of the all-electron mixed basis approach. Here I will show the result of the total energy, the ionization energy, and virial ratio for isolated atoms and dimers. In the third chapter, I describe the theory of LGW and the method to calculate the total energy based on the Luttinger–Ward functional within the plasmon-pole model proposed by von der Linden and Horsch. As a result, I confirm that the LGW improves the ionization potential, the electron affinity, and the total energy of atoms and dimers of lithium and sodium. In the fourth chapter, I will give the general theory, the relationship between Ward–Takahashi identity, and the implementation of GWΓ to our code in detail. I calculate the ionization potential and electron affinity for Li and Li_2 and optical absorption spectra for sodium clusters, and confirm the results are greatly improved compared to the GW and LGW. In the last chapter, I will make a brief concluding remarks for the GW, LGW, GWΓ approaches.

Chapter 2

GW Approximation with the All-Electron Mixed Basis Approach: Validity of Virial Theorem

2.1 Introduction

The validity of virial theorem plays a crucial role in first-principles calculations [17, 18]. In electronic systems, the total energy E is composed of kinetic energy T and potential energy V. The virial theorem asserts that $V = -2T$ under zero pressure. This is a very simple equation satisfied by every system that interacts only with Coulomb interactions. This theory is of course guaranteed not only in classical systems but also in quantum systems [19]. Therefore, it is desired to ensure virial theorem to be satisfied in the first-principles methods. It is well known that the Hartree–Fock (HF) approximation exactly satisfies virial theorem. It is also known that the local density approximation (LDA) of density functional theory (DFT) satisfies virial theorem, if the exchange-correlation energy is correctly divided into kinetic and potential energy contributions [20]. Also, there is a firm proof that all the theories in a conserving approximation exactly satisfies virial theorem.

On the basis of the many-body perturbation theory, Baym and Kadanoff [4] showed that the theory satisfies macroscopic conservation laws of energy, momentum, and angular momentum, if the corresponding theoretical system is represented in the following ways: (1) The Luttinger–Ward functional $\Phi[G]$ is approximately given by some limited sum of diagrams composed of Green's function G. (2) The self-energy is given by its functional derivative with respect to G, i.e., $\Sigma = \delta\Phi[G]/\delta G$. (3) Dyson's

equation with this self-energy Σ is solved self-consistently with respect to Green's function G. Such a theory is called a conserving approximation. One important point in this theory is that the total energy calculated from the Luttinger–Ward functional obeys a variational principle with respect to G [14]. Another important point is, as shown by Dahlen and van Leeuwen [5], that virial theorem holds exactly for a conserving approximation. Baym and Kadanoff [4] showed that the HF is a conserving approximation. The self-consistent GW approximation (GW) [3], which was called the shielding approximation in the paper by Baym and Kadanoff [4], is also a conserving approximation and satisfies virial theorem, it would give a good starting point for better approximations, as well as the HF.

The principal aim of this chapter is to confirm that virial theorem is surely satisfied in our code within the error of computational inaccuracies under the assumption that AOs are made by the atomic LDA calculation. Our targets are isolated closed-shell (noble gas and alkaline earth metal) atoms (He, Be, Ne, Mg, Ar, and Ca) [21] and some small clusters composed of nonmagnetic atoms which exhibit intrinsic spin magnetic moments [22]. It is very well known that O_2 has a spin-triplet ground state due to the degenerate bonding π orbitals at the Fermi level. Several other diatomic molecules such as B_2, Al_2, and Si_2 also have intrinsic spin magnetic moments. So far, the local density approximation (LDA) and the generalized gradient approximation (GGA) of density functional theory (DFT) have been applied to study the most stable spin states of small clusters and molecules [23]. In these approximations, however, the exchange interaction, which is very important as a major spin-dependent interaction, as well as the dynamically screened Coulomb interaction between electrons are not properly treated but drastically approximated as a function of only electron densities (and their derivatives in the GGA). The Hartree–Fock approximation (HFA), on the other hand, treats correctly the exchange interaction but does not take into account at all the electron correlation effect to screen this exchange interaction. One possible strategy to take into account both of these interactions is to invoke many-body perturbation theory and to use the GW approximation.

2.2 Theory

2.2.1 GW Approximation

The GW method was proposed by Hedin [3], in which the self-energy is expanded with Green's function G and the dynamically screened interaction W. The Green function in the many-body perturbation theory is given by

$$G(\boldsymbol{r}, t, \boldsymbol{r}', t') = i\langle T[\psi(\boldsymbol{r}, t)\psi^{\dagger}(\boldsymbol{r}', t')]\rangle, \tag{2.1}$$

where T and $\psi(\boldsymbol{r}, t)$ are the time-ordered operator and the field operator in the Hysenberg representation. The self-energy is an effective interaction from the virtual clouds surrounding a quasiparticle, and is defined as

$$\Sigma(\boldsymbol{r}, t, \boldsymbol{r}', t') = iG(\boldsymbol{r}, t, \boldsymbol{r}', t')W(\boldsymbol{r}, t, \boldsymbol{r}', t'). \tag{2.2}$$

The dynamically screened interaction is

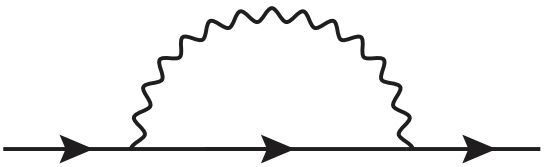

Fig.2.1: The Feynman diagrams of the self-energy The solid and wiggly lines show Green's function and the dynamically screened Coulomb interaction, respectively.

$$W(\boldsymbol{r}, t, \boldsymbol{r}', t') = \varepsilon(\boldsymbol{r}, t, \boldsymbol{r}', t')^{-1}v(\boldsymbol{r} - \boldsymbol{r}'), \tag{2.3}$$

where $\varepsilon(\boldsymbol{r}, t, \boldsymbol{r}', t')$ and $v(\boldsymbol{r} - \boldsymbol{r}') = 1/|\boldsymbol{r} - \boldsymbol{r}'|$ are the dielectric function and the bare Coulomb interaction. The dielectric function can be written as

$$\varepsilon(\boldsymbol{r}, t, \boldsymbol{r}', t') = 1 - \int v(\boldsymbol{r}, t, \boldsymbol{r}'', t'')P(\boldsymbol{r}'', t'', \boldsymbol{r}', t')d\boldsymbol{r}''dt, \tag{2.4}$$

where P is the polarization function. Within the random phase approximation (RPA), the polarization function can be written as

$$P(\boldsymbol{r}'', t'', \boldsymbol{r}', t') = -iG(\boldsymbol{r}'', t'', \boldsymbol{r}', t')G(\boldsymbol{r}', t', \boldsymbol{r}'', t''). \tag{2.5}$$

It is very convenient to consider the self-energy in Fourier space. The Fourier trans-

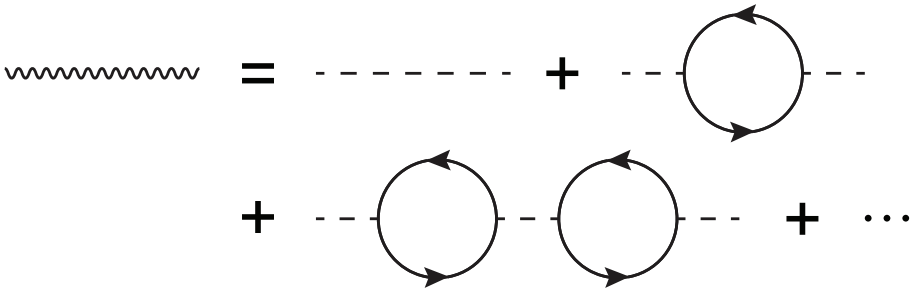

Fig.2.2: The Feynman diagrams of the dynamically screened Coulomb interaction.

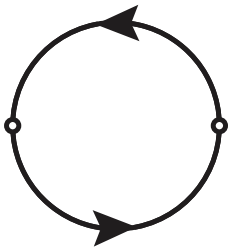

Fig.2.3: The Feynman diagrams of the polarization function.

form of Eqs.(2.1) and (2.2) are

$$G(\boldsymbol{r}, \boldsymbol{r}', \omega) = \sum_i \frac{\phi_i(\boldsymbol{r})\phi_i^*(\boldsymbol{r}')}{\omega - (\epsilon_i + i\eta_i)}, \tag{2.6}$$

$$\Sigma(\boldsymbol{r}, \boldsymbol{r}', \omega) = \frac{i}{2\pi} \int G(\boldsymbol{r}, \boldsymbol{r}', \omega - \omega')W(\boldsymbol{r}, \boldsymbol{r}', \omega')d\omega', \tag{2.7}$$

where, $\phi_i(\boldsymbol{r})$, ϵ_i are the quasiparticle wave function and energy, and η_i is a infinitesimal ($\eta_i = 0^+$ for occupied states and $\eta_i = 0^-$ for empty states). There are the following relation between the self-energy and Green's function:

$$G^{-1}(\boldsymbol{r}, \boldsymbol{r}', \omega) = G_0^{-1}(\boldsymbol{r}, \boldsymbol{r}', \omega) - \Sigma(\boldsymbol{r}, \boldsymbol{r}', \omega), \tag{2.8}$$

where G_0 is the non-interacting Green function. In the self-consistent GW, it is necessary to evaluate G, P, W, and Σ cyclically until the self-consistent solution is found. The schematic flow of the GW is shown in Fig.2.4. The self-consistency is a important point in the GW method, and there are three approaches. First one is called 1-shot GW (or G_0W_0), and it is widely used so far due to its simplicity. 1-shot GW is a non-self-consistent approach, and the quasiparticle wave function is not obtained. Within 1-shot GW, generally, the band gap or energy gap show good agreement with experimental data. Other two approaches are self-consistent approaches. One is the fully

self-consistent GW, and the other is called the partially self-consistent GW (or GW_0). The difference between them is the self-consistency for the dynamically screened interaction. In the GW_0, the dynamically screened interaction is represented by the polarization function constructed by G_0, i.e., the wave function obtained by the local density approximation (LDA) or the Hartree–Fock (HF) approximations. Here, we

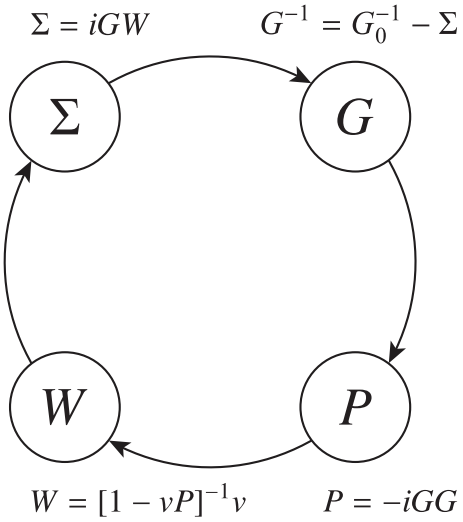

Fig.2.4: The schematic flow of the self-consistent GW approach.

must take the integration of ω' to evaluate Eq.(2.7) and this needs a lot of computational time. In order to avoid this frequency integration, the plasmon-pole model can be introduced. Some plasmon-pole models have been proposed so far [6, 24, 25]. In the generalized plasmon-pole model proposed by Hybertsen and Louie [6], the imaginary part of the inverse of the dielectric function can be approximately written as

$$\mathrm{Im}\varepsilon^{-1}_{\boldsymbol{G}\boldsymbol{G}'}(\omega) = A_{\boldsymbol{G}\boldsymbol{G}'}[\delta(\omega - \omega_{\boldsymbol{G}\boldsymbol{G}'}) - \delta(\omega + \omega_{\boldsymbol{G}\boldsymbol{G}'})], \tag{2.9}$$

where $\omega_{\boldsymbol{G}\boldsymbol{G}'}$ is the plasmon-pole frequency. Using the Kramers-Kronig relation, the real part of $\varepsilon^{-1}_{\boldsymbol{G},\boldsymbol{G}}(\omega)$ can be written as

$$\begin{aligned}\mathrm{Re}\varepsilon^{-1}_{\boldsymbol{G}\boldsymbol{G}'}(\omega) &= \delta_{\boldsymbol{G}\boldsymbol{G}'} - \frac{\mathrm{P}}{\pi}\int_{\infty}^{\infty}\frac{1}{\omega - \omega'}\mathrm{Im}\varepsilon^{-1}_{\boldsymbol{G}\boldsymbol{G}'}(\omega')d\omega' \\ &= \delta_{\boldsymbol{G}\boldsymbol{G}'} - \frac{2A_{\boldsymbol{G}\boldsymbol{G}'}}{\pi}\frac{\omega_{\boldsymbol{G}\boldsymbol{G}'}}{\omega^2 - \omega^2_{\boldsymbol{G}\boldsymbol{G}'}},\end{aligned} \tag{2.10}$$

where $A_{\boldsymbol{G}\boldsymbol{G}'}$ is determined to be satisfied with the f-sum rule:

$$A_{\boldsymbol{G}\boldsymbol{G}'} = -\frac{\pi}{2}\frac{\Omega^2_{\boldsymbol{G}\boldsymbol{G}'}}{\omega_{\boldsymbol{G}\boldsymbol{G}'}}, \tag{2.11}$$

where the effective bare plasma frequency, $\Omega^2_{\boldsymbol{G}\boldsymbol{G}'}$ is given by

$$\Omega^2_{\boldsymbol{G}\boldsymbol{G}'} = \omega^2_{pl} \frac{\boldsymbol{G}\cdot\boldsymbol{G}'}{|\boldsymbol{G}|^2} \frac{\rho(\boldsymbol{G}-\boldsymbol{G}')}{\rho(0)}. \tag{2.12}$$

Here, ω_{pl} is the plasma frequency defined as $\sqrt{4\pi\rho(0)}$. The plasmon-pole frequency, $\omega_{\boldsymbol{G}\boldsymbol{G}'}$ is obtained from the dielectric function in $\omega = 0$ limit:

$$\omega^2_{\boldsymbol{G}\boldsymbol{G}'} = \frac{\Omega^2_{\boldsymbol{G}\boldsymbol{G}'}}{\delta_{\boldsymbol{G}\boldsymbol{G}'} - \varepsilon^{-1}_{\boldsymbol{G}\boldsymbol{G}'}(\omega=0)}. \tag{2.13}$$

Using the generalized plasmon-pole model, we can write the dynamically screened interaction with $\Omega_{\boldsymbol{G},\boldsymbol{G}'}$ and $\omega_{\boldsymbol{G},\boldsymbol{G}'}$ as

$$W_{\boldsymbol{G}\boldsymbol{G}'}(\omega) = \varepsilon^{-1}_{\boldsymbol{G}\boldsymbol{G}'}(\omega) v(\boldsymbol{G}') = \delta_{\boldsymbol{G}\boldsymbol{G}'} v(\boldsymbol{G}') - \frac{\Omega^2_{\boldsymbol{G}\boldsymbol{G}'}}{\omega^2 - \omega^2_{\boldsymbol{G}\boldsymbol{G}'}} v(\boldsymbol{G}'). \tag{2.14}$$

Thus, the GW self-energy can be written as

$$\begin{aligned}(\nu|\Sigma_{\mathrm{GW}}(\omega)|\mu) &= \frac{i}{\Omega}\sum_i \sum_{\boldsymbol{G},\boldsymbol{G}'} \int \frac{d\omega'}{2\pi} \frac{(\nu|e^{i\boldsymbol{G}\cdot\boldsymbol{r}}|i\rangle\langle i|e^{-i\boldsymbol{G}'\cdot\boldsymbol{r}'}|\mu)}{\omega - \omega' - (\epsilon_i + i\eta_i)} W_{\boldsymbol{G},\boldsymbol{G}'}(\omega') \\ &= \frac{i}{\Omega}\sum_i \sum_{\boldsymbol{G},\boldsymbol{G}'} \int \frac{d\omega'}{2\pi} \frac{(\nu|e^{i\boldsymbol{G}\cdot\boldsymbol{r}}|i\rangle\langle i|e^{-i\boldsymbol{G}'\cdot\boldsymbol{r}'}|\mu)}{\omega - \omega' - (\epsilon_i + i\eta_i)} \qquad (2.15) \\ &\quad \times \left(\delta_{\boldsymbol{G}\boldsymbol{G}'} - \frac{\Omega^2_{\boldsymbol{G}\boldsymbol{G}'}}{\omega^2 - \omega^2_{\boldsymbol{G}\boldsymbol{G}'}}\right) v(\boldsymbol{G}'). \qquad (2.16)\end{aligned}$$

When we evaluate this self-energy in our self-consistent procedure, the computational cost is fairly large because the double summation for the reciprocal vectors $\boldsymbol{G}$, $\boldsymbol{G}'$. In order to reduce the computational cost further, we introduce the plasmon-pole model proposed by von der Linden and Horsch [25]. In the plasmon-pole model, the eigenvalue problem for the symmetrized dielectric function is solved:

$$v(\boldsymbol{G}) \sum_{\boldsymbol{G}'} \frac{|\boldsymbol{G}|}{|\boldsymbol{G}'|} P_{\boldsymbol{G}\boldsymbol{G}'}(\omega=0) u_p(\boldsymbol{G}') = \chi_p u_p(\boldsymbol{G}). \tag{2.17}$$

Note that in the original paper, the eigenvalue problem for the *inverse* of the symmetrized dielectric function is solved. The eigenvalue χ_p is related to the plasmon-pole strength z_p via

$$z_p = 1 - \frac{1}{1-\chi_p} = 1 - \lim_{\omega\to 0}\left[1 + \frac{z_p\omega_p^2}{\omega^2 - (\omega_p - i\eta)^2}\right]. \tag{2.18}$$

The plasmon-pole frequency ω_p is given by the relation

$$\omega_p^2 = \frac{4\pi}{z_p} \sum_{\boldsymbol{G},\boldsymbol{G}'} \Theta_p(\boldsymbol{G}) L_{\boldsymbol{G}\boldsymbol{G}'} \Theta_p(\boldsymbol{G}'), \tag{2.19}$$

where we put $L_{\boldsymbol{G}\boldsymbol{G}'} = (\boldsymbol{G}) \cdot (\boldsymbol{G}') n(\boldsymbol{G} - \boldsymbol{G}')$ and define the scaled plasmon-pole eigenvector as $\Theta_p(\boldsymbol{G}) = u_p(\boldsymbol{G})/|\boldsymbol{G}|$. The self-energy with the vdLH plasmon-pole model can be written as

$$\begin{aligned}(\nu|\Sigma_{\mathrm{GW}}(\omega)|\mu) = \frac{i}{\Omega} \sum_i \sum_{\boldsymbol{G},\boldsymbol{G}'} \int \frac{d\omega'}{2\pi} \frac{(\nu|e^{i\boldsymbol{G}\cdot\boldsymbol{r}}|i\rangle\langle i|e^{-i\boldsymbol{G}'\cdot\boldsymbol{r}'}|\mu)}{(\omega - \omega' - (\epsilon_i + i\eta_i))} \\ \times \left(\delta_{\boldsymbol{G},\boldsymbol{G}'} v(\boldsymbol{G}') + \sum_p \frac{4\pi z_p \omega_p^2}{\omega'^2 - (\omega_p - i\eta)^2} \Theta_p(\boldsymbol{G}) \Theta_p^*(\boldsymbol{G}')\right),\end{aligned} \tag{2.20}$$

where η is a positive infinitesimal. We can divide this self-energy into two terms, i.e., the Fock exchange (Σ_{x}) and the correlation (Σ_{c}) terms:

$$(\nu|\Sigma_{\mathrm{x}}|\mu) = -\frac{1}{\Omega} \sum_i^{\mathrm{occ}} \sum_{\boldsymbol{G}} (\nu|e^{i\boldsymbol{G}\cdot\boldsymbol{r}}|i\rangle\langle i|e^{-i\boldsymbol{G}\cdot\boldsymbol{r}'}|\mu) v(\boldsymbol{G}) \tag{2.21}$$

and

$$\begin{aligned}(\nu|\Sigma_{\mathrm{c}}(\omega)|\mu) &= \frac{i}{\Omega} \sum_i \sum_{\boldsymbol{G},\boldsymbol{G}'} \sum_p 4\pi z_p \omega_p^2 \\ &\quad \times \int \frac{d\omega'}{2\pi} \frac{\Theta_p(\boldsymbol{G})(\nu|e^{i\boldsymbol{G}\cdot\boldsymbol{r}}|i\rangle\langle i|e^{-i\boldsymbol{G}'\cdot\boldsymbol{r}'}|\mu)\Theta_p^*(\boldsymbol{G}')}{(\omega - \omega' - (\epsilon_i + i\eta_i))(\omega'^2 - (\omega_p - i\eta)^2)} \\ &= \frac{2\pi}{\Omega} \sum_p z_p \omega_p^2 \Bigg(\sum_i^{\mathrm{occ}} \frac{\beta_p^{\nu\, i} [\beta_p^{\mu\, i}]^*}{\omega - (E_i + i\eta) + (\omega_p - i\eta)} \qquad (2.22) \\ &\qquad + \sum_i^{\mathrm{emp}} \frac{\beta_p^{\nu\, i} [\beta_p^{\mu\, i}]^*}{\omega - (E_i - i\eta) - (\omega_p - i\eta)} \Bigg), \qquad (2.23)\end{aligned}$$

where

$$\beta_p^{\nu\, i} = \sum_{\boldsymbol{G}} \Theta_p(\boldsymbol{G}) (\nu|e^{i\boldsymbol{G}\cdot\boldsymbol{r}}|i\rangle. \tag{2.24}$$

2.2.2 Total Energy

In the LDA, the Kohn–Sham eigenstates $|\nu\rangle$ and eigen-energies ε_ν are obtained by solving the Kohn–Sham equation

$$\left[\hat{T} + \hat{v}_{\mathrm{nuc}} + \hat{v}_{\mathrm{H}} + \mu_{\mathrm{xc}}(n)\right] |\nu\rangle \;=\; \varepsilon_\nu |\nu\rangle, \tag{2.25}$$

where $\hat{T}$, $\hat{v}_{\rm nuc}$, and $\hat{v}_{\rm H}$ are the kinetic energy operator, local potential due to nucleus, and the Hartree potential, respectively; $n = n(\boldsymbol{r})$ is the electron density, and $\mu_{\rm xc}(n)$ is the local exchange-correlation potential, which is related to the local exchange-correlation energy $\varepsilon_{\rm xc}(n)$ via the relation $\mu_{\rm xc}(n) = (d/dn)n\varepsilon_{\rm xc}(n)$. The exchange-correlation energy, $E_{\rm xc} = \int d\boldsymbol{r} n(\boldsymbol{r})\varepsilon_{\rm xc}(n(\boldsymbol{r}))$, is divided into a kinetic energy part $T_{\rm xc}$ and a potential energy part $U_{\rm xc}$. According to Averill and Painter [20], $T_{\rm xc}$ is given by

$$T_{\rm xc} = \int d\boldsymbol{r} n(\boldsymbol{r})[3\mu_{\rm xc}(n(\boldsymbol{r})) - 4\varepsilon_{\rm xc}(n(\boldsymbol{r}))]. \tag{2.26}$$

Then the true kinetic-energy and potential-energy contributions to the ground-state total energy is given by $T = T_{\rm s}+T_{\rm xc}$ and $V = V_{\text{n-e}}+V_{\rm H}+E_{\rm xc}-T_{\rm xc} = V_{\text{n-e}}+V_{\rm H}-3V_{\rm xc}+5E_{\rm xc}$, respectively. Here, $T_{\rm s}$ is the kinetic-energy of a non-interacting system and $V_{\rm xc}$ is the exchange-correlation potential defined as $V_{\rm xc} = \int d\boldsymbol{r} n(\boldsymbol{r})\mu_{\rm xc}(n(\boldsymbol{r}))$.

On the other hand, in many-body perturbation theory, the quasiparticle equation, which is equivalent to Dyson's equation, is generally written as

$$\left[\hat{T} + \hat{v}_{\rm nuc} + \Sigma(\varepsilon_\nu)\right]|\nu\rangle \;=\; \varepsilon_\nu|\nu\rangle, \tag{2.27}$$

where $\Sigma(\varepsilon_\nu)$ is the self-energy operator. The self-energy is composed of three parts: the Hartree potential given by $\hat{v}_{\rm H}(\boldsymbol{r}) = \int d\boldsymbol{r}' n(\boldsymbol{r}')/|\boldsymbol{r}-\boldsymbol{r}'|$, the exchange part given by $\Sigma_{\rm x}(\boldsymbol{r},\boldsymbol{r}') = -\sum_\lambda^{\rm occ}\phi_\lambda(\boldsymbol{r})\phi_\lambda^*(\boldsymbol{r}')/|\boldsymbol{r}-\boldsymbol{r}'|$, and the correlation part $\Sigma_{\rm c}(\boldsymbol{r},\boldsymbol{r}';\varepsilon_\nu) = \langle\boldsymbol{r}|\Sigma_{\rm c}(\varepsilon_\nu)|\boldsymbol{r}'\rangle$, in the coordinate representation (we put the quasiparticle wave functions $\phi_\lambda(\boldsymbol{r}) = \langle\boldsymbol{r}|\lambda\rangle$). To avoid the difficulty of the energy dependence in the self-energy, we simply replace its ε_ν with $\omega_0 = (\varepsilon_{\rm HOMO} + \varepsilon_{\rm LUMO})/2$ (for He, we use $\omega_0 = \varepsilon_{\rm HOMO}$) in this thesis. Here HOMO and LUMO mean the highest occupied and lowest unoccupied molecular orbitals, respectively. Then, substituting Eq.(2.39) in Eq.(2.27) and multiplying $(\xi'|$ from the left in the both sides of the equation, we obtain the generalized eigenvalue equation:

$$\sum_\xi(\xi'|\hat{T} + \hat{v}_{\rm nuc} + \Sigma(\omega_0)|\xi)c_\nu(\xi) = \varepsilon_\nu\sum_\xi(\xi'|\xi)c_\nu(\xi), \tag{2.28}$$

where $(\xi'|\xi) = S_{\xi'\xi}$ is an overlap matrix. Equation (2.28) can be transformed to the ordinary eigenvalue equation by using the Choleski decomposition as in the case of the LDA calculation [26]. The quasiparticle states and the quasiparticle energies are obtained by solving this generalized eigenvalue problem self-consistently.

In the HF and GW, the electron density is given by

$$\begin{aligned} n(\boldsymbol{r}) &= \langle \Psi_{\mathrm{G}}^N | \hat{\psi}^\dagger(\boldsymbol{r}) \hat{\psi}(\boldsymbol{r}) | \Psi_{\mathrm{G}}^N \rangle \\ &= \sum_\nu \langle \Psi_{\mathrm{G}}^N | \hat{\psi}^\dagger(\boldsymbol{r}) | \Psi_\nu^{N-1} \rangle \langle \Psi_\nu^{N-1} | \hat{\psi}(\boldsymbol{r}) | \Psi_{\mathrm{G}}^N \rangle \\ &= \sum_\nu^{\mathrm{occ}} \phi_\nu^*(\boldsymbol{r}) \phi_\nu(\boldsymbol{r}), \end{aligned} \tag{2.29}$$

and the total kinetic energy is estimated as

$$\begin{aligned} T &= \langle \Psi_{\mathrm{G}}^N | \hat{T} | \Psi_{\mathrm{G}}^N \rangle \\ &= \langle \Psi_{\mathrm{G}}^N | \left(-\frac{1}{2} \int d\boldsymbol{r} \hat{\psi}^\dagger(\boldsymbol{r}) \nabla^2 \hat{\psi}(\boldsymbol{r}) \right) | \Psi_{\mathrm{G}}^N \rangle \\ &= -\frac{1}{2} \sum_\nu \int d\boldsymbol{r} \langle \Psi_{\mathrm{G}}^N | \hat{\psi}^\dagger(\boldsymbol{r}) | \Psi_\nu^{N-1} \rangle \langle \Psi_\nu^{N-1} | \nabla^2 \hat{\psi}(\boldsymbol{r}) | \Psi_{\mathrm{G}}^N \rangle \\ &= -\frac{1}{2} \sum_\nu^{\mathrm{occ}} \int d\boldsymbol{r} \phi_\nu^*(\boldsymbol{r}) \nabla^2 \phi_\nu(\boldsymbol{r}), \end{aligned} \tag{2.30}$$

where $\hat{\psi}^\dagger(\boldsymbol{r})$ and $\hat{\psi}(\boldsymbol{r})$ are the creation and annihilation operators; $|\Psi_{\mathrm{G}}^N\rangle$ and $|\Psi_\nu^{N-1}\rangle$ are the N-electron ground state and the ν-th $(N-1)$-electron states, respectively. Note that there is only a limited number of the bound $(N-1)$-electron states, which is equal to N accounting for spin duplicity in a system having N protons, and we take into account these bound states only in the intermediate states. Similarly, the total energy contributions from the nuclear-electron Coulomb potential, the Hartree potential, the Fock exchange energy, and the correlation energy are estimated as

$$V_{\text{n-e}} = \sum_\nu^{\mathrm{occ}} \int d\boldsymbol{r} \psi_\nu^*(\boldsymbol{r}) v_{\mathrm{nuc}}(\boldsymbol{r}) \psi_\nu(\boldsymbol{r}) \tag{2.31}$$

$$= -\sum_\nu^{\mathrm{occ}} \sum_\alpha \int d\boldsymbol{r} \psi_\nu^*(\boldsymbol{r}) \frac{Z_\alpha}{|\boldsymbol{r} - \boldsymbol{R}_\alpha|} \psi_\nu(\boldsymbol{r}), \tag{2.32}$$

$$V_{\mathrm{H}} = \frac{1}{2} \sum_\nu^{\mathrm{occ}} \int d\boldsymbol{r} \psi_\nu^*(\boldsymbol{r}) v_{\mathrm{H}}(\boldsymbol{r}) \psi_\nu(\boldsymbol{r}), \tag{2.33}$$

$$V_{\mathrm{x}} = \frac{1}{2} \sum_\nu^{\mathrm{occ}} \int d\boldsymbol{r} d\boldsymbol{r}' \psi_\nu^*(\boldsymbol{r}) \Sigma_{\mathrm{x}}(\boldsymbol{r}, \boldsymbol{r}') \psi_\nu(\boldsymbol{r}'), \tag{2.34}$$

$$\begin{aligned} \Phi_{\mathrm{c}}[G] &= -\frac{1}{2} \lim_{\lambda \to 1} \sum_{n=1}^\infty \frac{\lambda^n}{n} \mathrm{Tr} \left[\Sigma_{\mathrm{c}}^{(n)}[G] \, G \right] \\ &= -\frac{1}{2} \int_0^1 \frac{d\lambda}{\lambda} \mathrm{Tr} \left[\sum_{n=1}^\infty \lambda^n \Sigma_{\mathrm{c}}^{(n)}[G] \, G \right], \end{aligned} \tag{2.35}$$

where $\Phi_c[G]$ is the correlation part of the Luttinger–Ward functional [14,15], $\Sigma_c^{(n)}[G]$ is the correlation part of the self-energy composed of the n-th order skeleton diagrams, and G is Green's function. Thus the total potential energy is given by $V = V_{\text{n-e}} + V_{\text{H}} + V_{\text{x}} + \Phi_c$.

The correlation part of the Luttinger–Ward functional can be given by

$$\Phi_c[G] = -\frac{2\pi i}{\Omega}\sum_{\nu}\sum_{\nu'}\sum_{p}\frac{1}{2}\int_0^1\frac{d\lambda}{\lambda}\int_{-\infty}^{\infty}\frac{d\omega}{2\pi}\frac{e^{i\eta\omega}}{\omega-\epsilon_\nu-i\eta_\nu} \tag{2.36}$$

$$\times\frac{\lambda z_p(\lambda)\omega_p(\lambda)[M_p^{\nu'\nu}]^* M_p^{\nu'\nu}}{\omega-\epsilon_{\nu'}+\omega_p(\lambda)\mathrm{sgn}(\mu-\epsilon_{\nu'})-i\eta_{\nu'}}$$

$$= \frac{2\pi}{\Omega}\sum_{\nu}^{\text{occ}}\sum_{\nu'}^{\text{emp}}\sum_{p}\frac{1}{2}\int_0^1 d\lambda\frac{z_p(\lambda)\omega_p(\lambda)[M_p^{\nu'\nu}]^* M_p^{\nu'\nu}}{\epsilon_\nu-\epsilon_{\nu'}+\omega_p(\lambda)\mathrm{sgn}(\mu-\epsilon_{\nu'})+i\eta}$$

$$-\frac{2\pi}{\Omega}\sum_{\nu}^{\text{emp}}\sum_{\nu'}^{\text{occ}}\sum_{p}\frac{1}{2}\int_0^1 d\lambda\frac{z_p(\lambda)\omega_p(\lambda)[M_p^{\nu'\nu}]^* M_p^{\nu'\nu}}{\epsilon_\nu-\epsilon_{\nu'}+\omega_p(\lambda)\mathrm{sgn}(\mu-\epsilon_{\nu'})-i\eta}, \tag{2.37}$$

where we put

$$M_p^{\nu'\nu} = \sum_{\boldsymbol{G}}\langle\,\nu'\,|\,e^{-i\boldsymbol{G}\cdot\boldsymbol{r}}\,|\,\nu\,\rangle\Theta_p^*(\boldsymbol{G}). \tag{2.38}$$

The λ-dependent plasmon-pole frequency $\omega_p(\lambda)$ and plasmon-pole strength $z_p(\lambda)$ are analogues of the λ-indepenent ones defined in Ref. [27]. The λ integral in Eq.(3.30) can be performed analytically. In the next chapter, we describe the Luttinger–Ward functional and the λ-dependent plasmon-pole model in detail.

2.3 Methodology

2.3.1 All-Electron Mixed Basis Approach

In the all-electron mixed basis approach, the Kohn–Sham or quasiparticle states are expressed as a linear combination of atomic orbital (AO) and plane wave (PW) basis functions:

$$|\nu\rangle = \sum_{\boldsymbol{G}} c_\nu(\boldsymbol{G})|\boldsymbol{G}) + \sum_{jnlm} c_\nu(jnlm)|jnlm)$$

$$= \sum_{\xi} c_\nu(\xi)|\xi), \tag{2.39}$$

where $\boldsymbol{G}$'s denote reciprocal lattice vectors, and j, n, l, and m are the atom index, the principal quantum number, the angular momentum quantum number, and the index

for the cubic harmonics. AOs are numerically generated by the Herman–Skillman [28] type atomic code in a logarithmic radial mesh with the same LDA functional [29] as that used in our all-electron mixed basis code.

We use a spherical cut-off technique truncating the Coulomb interaction to avoid the effect of neighbouring unit cells [30]. We use the fcc unit cell of edge length 10 Å for He, 12 Å for the other isolated atoms, and 16 Å for the dimers. and use 13.38 (for He), 9.29 (for the other isolated atoms), and 5.23 (for the dimers) Ry cut-off energies for PWs and the correlation part of the self-energy, and 99.50 (for He), 44.22 (for the other isolated atoms), and 24.87 (for the dimers) Ry cut-off energies for the exchange part of the self-energy. For PWs, we use the fast Fourier transformation (FFT) dividing the unit cell by 192×192×192. For the AOs, we use all the core and valence AOs in the calculation, although the valence AOs are confined inside the atomic sphere of radius 4 Bohr (2.1167 Å) by subtracting a smooth parabolic function that satisfies the matching condition on the atomic sphere. Then, this parabolic function smoothly connecting to the true AO outside the atomic sphere can be well represented by a linear combination of PWs in Eq. (2.39). For each dimer, we compare the total energies of the singlet and triplet states at the same bond length, because we want to avoid any complication caused by the difference of the dimer structure in our discussion. Therefore, in our study, the bond length is fixed at an optimized value for the triplet state determined by the LDA calculation using the DMol^3 package program [31, 32] in Materials Studio; 1.614 Å, 2.453 Å, and 2.151 Å for B_2, Al_2, and Si_2, respectively. We have checked that the total energy is almost flat (maximum change in the energy is only about 0.045 eV) within ±0.05 Å around the assumed bond length both for the triplet and singlet states, and that virial theorem under zero pressure is well guaranteed in our system.

2.4 Results and Discussion

2.4.1 Isolated Atoms

The total energy E_{G}^{N}, its components (T, $V_{\text{n-e}}$, V_{H}, E_{xc} / V_{x}, and V_{xc} / Φ_{c}), and virial ratio of He, Be, Ne, Mg, Ar, and Ca are summarized in Table.2.1. Virial ratio of the LDA is strikingly almost perfectly equal to 2 for all elements, and virial ratios of the HF and GW are also almost 2, although little bit off from the exact value 2. The reason of this inaccuracy in our HF and GW calculations is that AOs are generated by the

atomic (Herman–Skillman-type) LDA code; they are not necessarily conformable to the AOs of the HF or GW. In this sense, the quasiparticle wave functions are described with slightly worse basis set in the HF and GW than in the LDA. In the HF, if we use the AOs generated by an atomic HF calculation code [33], our results for virial ratio become in fact drastically improved: we obtained the excellent values 1.999938 for He and 2.000005 for Be in our all-electron mixed basis code. On the other hand, in the LDA, if we use the original energy division, $T_s \rightarrow T$ and $V_{n\text{-}e} + V_H + E_{xc} \rightarrow V$, virial ratio becomes somewhat worse: 2.0249 for He, 2.0096 for Be, and 2.0040 for Ne, 2.0023 for Mg, 2.0019 for Ar, and 2.0016 for Ca.

For all atomic species, as expected, the absolute value of the total energy of the GW is larger than that of the HF, and is almost the same as that of the HF plus the correlation energy (Φ_c), although it is interesting to note that the total energy components are significantly different between the HF and GW results, i.e., these differences are much larger than Φ_c.

The eigenvalues of the HOMO and LUMO levels are summarized in Table.2.2 as well as the available experimental data [34–40]. The minus of these energies corresponds to the ionization potential (IP) and electron affinity (EA). In the last column (LUMO of Expt.) of this table, – means a negative EA [41]. The results of the LDA (even for the HOMO level) are not comparable to the experimental data, although Janak's theorem is known to hold for the HOMO level in the exact DFT [15]. This is because the LDA is not the exact DFT. The absolute value of the HOMO energy of the HF overestimates the experimental IP for noble gases and underestimates it for Be and Mg, while that of the GW is in excellent agreement with the experimental IP for all elements. The LUMO energy of the GW is smaller than that of the HF, reflecting the fact that the energy gap is generally overestimated in the HF.

For He, Be, and Mg, the positive LUMO energies are consistent with the negative EA in the experiments. For Ne and Ar, the LUMO energies obtained by the GW are slightly below the vacuum level, although they should correspond to the negative EA. In our all-electron mixed basis calculation, however, even if the LUMO quasiparticle energy is negative, the calculated LUMO level may correspond to a resonating virtual bound state [42], which have a large amplitude around the atom and continuously continues to a PW far apart from the atom. The LUMO quasiparticle wave functions of He, Ne, and Ar calculated by the GW are shown in Fig.2.5 in an isosurface view. The graphics of the wave functions are generated with Materials Studio provided. They all spread out in the unit cell, and apparently correspond to resonating virtual

Table.2.1: Total energy, its components in a.u., and virial ratio ($-V/T$). In the components, T is the kinetic energy given by T_s + T_{xc} in the LDA (see Eq. (2.26)) or by Eq. (2.30) in the HF and GW, $V_{n\text{-}e}$ is the nucleus-electron Coulomb energy, V_H is the Hartree energy, E_{xc} is the LDA exchange-correlation energy including T_{xc} given by Eq. (2.26), V_x is the Fock exchange energy in the HF and GW, V_{xc} is the LDA exchange-correlation potential, and Φ_c is the correlation energy in the case of the GW.

		E_G^N	T	$V_{n\text{-}e}$	V_H	E_{xc} / V_x	V_{xc} / Φ_c	$-V/T$
	LDA	−2.8344	2.8348	−6.6240	1.9953	−0.9725	−1.2740	1.9998
He	HF	−2.8616	2.8639	−6.7511	2.0511	−1.0256	–	1.9992
	GW	−2.8958	2.7869	−6.6555	2.0155	−1.0077	−0.0350	2.0391
	LDA	−14.4463	14.4467	−33.3561	7.1140	−2.5138	−3.3060	2.0000
Be	HF	−14.5728	14.5731	−33.6325	7.1517	−2.6650	–	2.0000
	GW	−14.6166	14.5890	−33.6715	7.1804	−2.6704	−0.0441	2.0019
	LDA	−128.2280	128.2139	−309.9639	65.7176	−11.7040	−15.4414	2.0001
Ne	HF	−128.5414	128.1462	−310.7470	66.1422	−12.0828	–	2.0031
	GW	−128.6087	127.9716	−310.3223	65.8538	−12.0407	−0.0710	2.0050
	LDA	−199.1340	199.1300	−477.8793	95.6547	−15.4482	−20.4005	2.0000
Mg	HF	−199.6069	199.2132	−478.6790	95.8478	−15.9708	–	2.0020
	GW	−199.6424	199.2118	−478.7424	95.8966	−15.9726	−0.0358	2.0022
	LDA	−525.9396	525.9131	−1253.0800	231.4329	−29.2340	−38.6549	2.0001
Ar	HF	−526.8091	526.1114	−1254.4943	231.7399	−30.1661	–	2.0013
	GW	−526.9716	525.5884	−1253.4500	231.1687	−30.1122	−0.1674	2.0026
	LDA	−675.7430	675.7085	−1601.3530	285.1102	−34.1292	−45.1467	2.0001
Ca	HF	−676.7603	675.7283	−1602.1591	284.8580	−35.1747	–	2.0015
	GW	−676.7899	675.6615	−1602.0841	284.8330	−35.1705	−0.0298	2.0017

bound states; note that because of the fcc unit cell, the spherical wave is folded at the cell surfaces.

In a detailed analysis of noble gas atoms, we found that the LUMO wave functions of the GW spread wider than that of the LDA and thinner than that of the HF. For example, for He, the LUMO wave function of the GW, Fig.2.5(a), is depicted at the isosurface value of 0.36, while similar profiles in the LUMO wave functions of the LDA (Fig.2.6) and HF (Fig.2.7) appear at the isosurface values of 0.23 and 0.50, respectively. (The units are such that the isosurface value of unity corresponds to the wave function everywhere flat inside the fcc unit cell.) The isosurface values are therefore LDA < GW < HF, which indicates the above-mentioned tendency.

If we enlarge the unit cell of the system, the PW region becomes larger than the atomic region, and thus the relative norm of the PW part of the LUMO wave func-

tion becomes dominant and the relative norm of the atomic localized part becomes negligible. In fact, for Ar, if we enlarge the unit cell size from 12 Å to 14 Å and 16 Å using the same cut off energies, the PW region enlarges and the atomic region shrinks, resulting in the LUMO energy changing from the value −0.1919 eV listed in Table.2.2 to −0.1427 eV and −0.1046 eV, asymptotically approaching to +0.157 eV (see Fig.2.8) in the HF, while the change of HOMO energy is negligibly small compared to that of the LUMO energy. (Note that this kind of calculation is only possible in the all-electron mixed basis approach, because it can handle a PW-like state of an isolated atom in an all-electron formalism and determine its absolute energy value.) That is, if there is an isolated atom in an infinite vacuum space, the wave function becomes a pure PW that resonates with the atomic part. Therefore, our result for the positive LUMO level is reasonable (even if it is negative, it is acceptable) in a sense that it may become some positive value by an extrapolation to the infinite unit cell size, although we have not done this extrapolation for every case because this is not the main purpose of this thesis. It would be interesting in the future to compare such extrapolated data with the old experimental data [41].

Typically, the self-consistent GW has a tendency to overestimate the energy gap. However, the energy gap of Ca obtained by the GW is very slightly underestimated compared to the experimental data. We think that this is an exceptional case. In fact, we obtained the GW energy gap, which is larger than experimental values, for Li_2 and Na_2 clusters [43]. Anyway, in order to improve the GW result, the vertex correction [3] should be taken into account. Such a work is left for the future study.

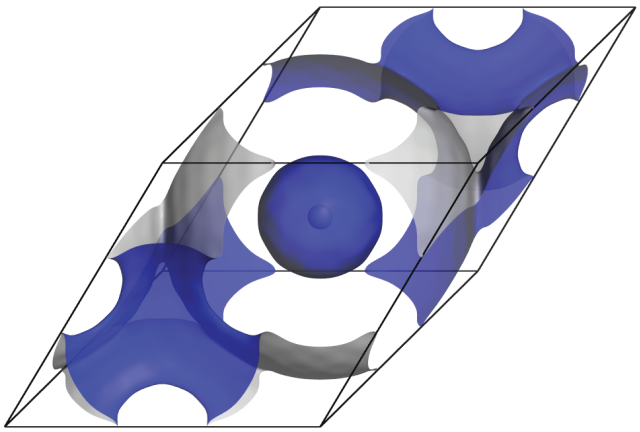

Fig.2.6: The Kohn–Sham (LDA) wave function of the LUMO level of He. The isosurface value is 0.23.

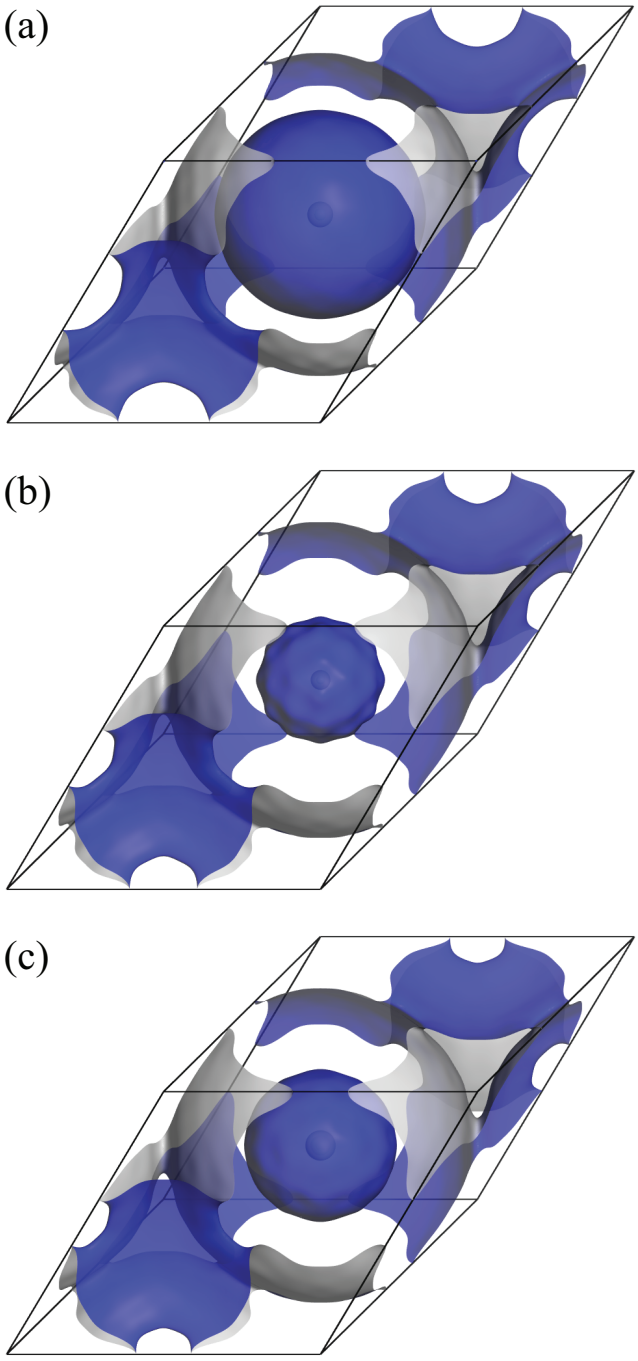

Fig.2.5: The GW quasiparticle wave function of the LUMO level of (a) He, (b) Ne, and (c) Ar. The atom is located at the center of the fcc unit cell. The isosurface values are 0.36, 0.39, and 0.47, respectively. Here and hereafter, the isosurface value of unity corresponds to the (normalized) wave function everywhere flat inside the fcc unit cell.

Table.2.2: Eigenvalues of the HOMO and LUMO levels in eV obtained by the LDA, HF and GW calculations. The minus of the experimental IP corresponding to HOMO and the minus of the experimental EA corresponding to LUMO ("–" means a negative EA [41]) are also listed in the last column (Expt.) for comparison.

	LDA		HF		GW		Expt.	
	HOMO	LUMO	HOMO	LUMO	HOMO	LUMO	HOMO	LUMO
He	−15.5114	−0.1136	−24.9711	0.0932	−24.5707	0.0789	−24.587[a]	–
Be	−5.6103	−1.8207	−8.4134	0.2142	−9.3187	0.1110	−9.3227[b]	–
Ne	−13.5402	−0.2886	−23.1354	0.0078	−21.5566	−0.0123	−21.5645[c]	–
Mg	−4.8084	−1.4321	−6.8915	0.2369	−7.6666	0.08264	−7.646[d]	–
Ar	−10.3988	−0.6383	−16.0671	−0.1919	−15.1695	−0.2453	−15.7596[e]	–
Ca	−3.9701	−1.6442	−5.4067	0.1717	−6.0776	−0.1701	−6.113[f]	−0.043±0.007[g]

[a] See Ref. [34]
[b] See Ref. [35]
[c] See Ref. [36]
[d] See Ref. [37]
[e] See Ref. [38]
[f] See Ref. [39]
[g] See Ref. [40]

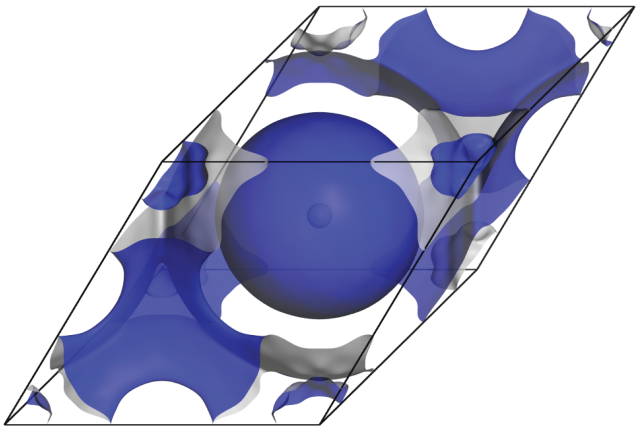

Fig.2.7: The HF quasiparticle wave function of LUMO level of He. The isosurface value is 0.50.

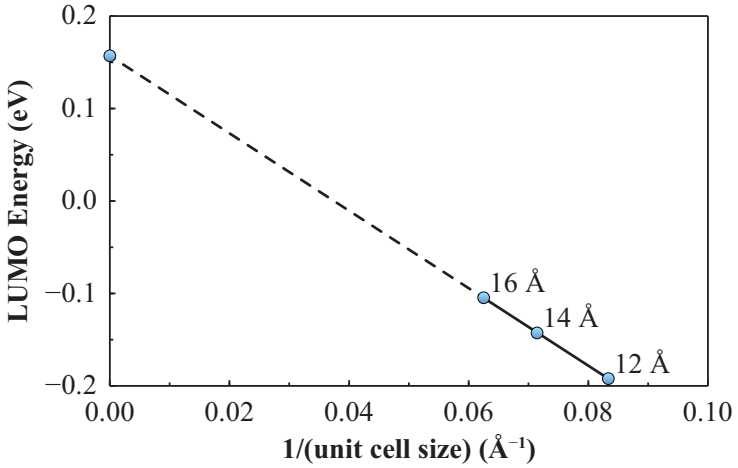

Fig.2.8: The LUMO energy (in eV) of Ar estimated by the HF versus the inverse of the unit cell size (in $Å^{-1}$) and its extrapolation to the infinite unit cell size.

2.4.2 Spin polarized dimers

The total energy E_G^N and its components (T, $V_{n\text{-}e}$, V_H, V_x, and Φ_c) as well as virial ratio of B_2, Al_2, and Si_2 are summarized in Table.2.3 for both singlet and triplet states. As seen from Table.2.3, the total energy of the triplet state is lower than the total energy of the singlet state. The triplet-singlet energy difference is 0.25 eV, 0.16 eV, and 0.20 eV, respectively, for B_2, Al_2, and Si_2. The exchange-correlation energy, $V_x + \Phi_c$, is all negative, and has larger absolute values for the triplet state than for the singlet state. The difference in the exchange-correlation energy, $V_x + \Phi_c$, between the triplet and singlet states is 0.23 eV, 0.07 eV, and 1.00 eV, respectively, for B_2, Al_2, and Si_2. These values roughly correspond to the total energy difference between the triplet and singlet states written above. Such a correspondence is not observed, however, in all the other contributions (T, $V_{n\text{-}e}$, and V_H); the sign in the difference in each contribution between the triplet and singlet states is the same among B_2 and Al_2, but different from Si_2.

Virial ratio is within the error of 0.5 % for B_2 and 0.1 % for Al_2 and Si_2. These values are at a first glance not acceptable to guarantee the accuracy of the total energy of

Table.2.3: Total energy and its components in Hartree as well as virial ratio ($-V/T$). In the components, T is the kinetic energy, $V_{\text{n-e}}$ is the nucleus-electron Coulomb energy, V_{H} is the Hartree energy, V_{x} is the Fock exchange energy, and Φ_{c} is the correlation energy.

		E_{G}^{N}	T	$V_{\text{n-e}}$	V_{H}	V_{x}	Φ_{c}	$-V/T$
B_2	Singlet	−49.1638	48.6847	−126.4018	29.3884	−7.4439	−0.1548	2.010
	Triplet	−49.1730	48.6877	−126.4079	29.4079	−7.4558	−0.1516	2.010
Al_2	Singlet	−483.8782	482.8470	−1184.4510	239.8146	−36.1241	−0.1432	2.002
	Triplet	−483.8840	482.8405	−1184.4662	239.8309	−36.1290	−0.1409	2.002
Si_2	Singlet	−577.8886	576.5609	−1423.6989	286.8815	−40.5261	−0.1889	2.002
	Triplet	−577.8963	576.3775	−1423.4503	286.6898	−40.4778	−0.2003	2.003

order −578 Hartree (of Si_2) in the discussion of the total energy difference of order 0.2 eV. However, this inaccuracy is mainly caused by the usage of the AOs determined by the Herman–Skillman-type atomic LDA code. If we could use the GWA-based AOs instead of the LDA-based AOs, virial ratio would become much closer to the exact value 2. This can be seen, for example, from the fact that, if we use the atomic HFA code in place of the atomic LDA code to determine the AOs, the resulting virial ratio of the all-electron mixed basis HFA calculation improves from 1.9992 to 1.999938 [21]. Therefore, this inaccuracy in the present calculation mainly affects to the calculation of core states only, because the valence AOs can be well supplemented by the PWs but the very localized core AOs cannot be supplemented so much by the PWs, i.e., the core states are described by slightly worse basis functions. Therefore, we can expect one order higher accuracy if we could exclude the core contribution from the total energy.

We find that the kinetic energy contribution from the core states (1s-2p) of Si_2 is 566.9033 Hartree for the singlet state and 566.9397 Hartree for the triplet state, and their difference is only 0.0364 Hartree, which is much smaller than the difference 0.1834 Hartree in the total kinetic energies (576.5609 and 576.3775 Hartree) given in Table.2.3 This suggests that, because the total energy difference between the singlet and triplet states is 0.2 eV, its core component in the difference would be estimated as 0.004 eV, which is a negligible order in our discussion. Therefore, we can subtract the core contribution from the total energy and discuss its residue only. Since the core contribution is 566.9033/576.5609 = 98.32 % of the total energy, just 1.68 % of the total energy, i.e., 9.7 Hartree for Si_2, is this residue. Since one order higher accuracy is expected for virial ratio in this residue, i.e. the relative error is estimated as 0.01 %,

the error in this residue is estimated to be 0.00097 Hartree, which is equal to 0.026 eV. Thus we can conclude that the present calculation has an enough accuracy to discuss the total energy difference of the order of 0.2 eV.

The eigenvalues of the HOMO and LUMO levels calculated with the GWA are summarized in Table.2.4 as well as the available experimental data [44–49]. The minus of these energies corresponds to the ionization potential (IP) and electron affinity (EA). The results are fairly in good agreement with the experimental data, although they have a common tendency to overestimate the experimental energy gap.

Table.2.4: Eigenvalues of the HOMO and LUMO levels in eV obtained by the GWA calculation. The minus of the experimental IP corresponding to HOMO and the minus of the experimental EA corresponding to LUMO are also listed in the last column (Expt.) for comparison.

		GWA	Expt.
B_2	HOMO	−9.698	−10.30[a]
	LUMO	−1.827	$> -1.3 \pm 0.4$[b]
Al_2	HOMO	−6.886	-5.4 ± 1.0[c]
	LUMO	−1.392	-1.460 ± 0.060[d]
Si_2	HOMO	−8.642	−7.9[e]
	LUMO	−1.881	-2.230 ± 0.010[f]

[a] See Ref. [44].
[b] See Ref. [45].
[c] See Ref. [46].
[d] See Ref. [47].
[e] See Ref. [48].
[f] See Ref. [49].

In Fig.2.9, we show the quasiparticle energy spectra for the triplet state calculated by our GWA calculation. Here, the quasiparticle energies mean the total energy difference between the N-electron ground state and the $(N \pm 1)$-electron excited states. In this figure, the levels with up and down arrows (indicating electron spins) denote hole (occupied) levels and those without arrows denote electron (unoccupied) levels. The topmost level with an arrow corresponds to the HOMO level and the lowermost level without an arrow corresponds to the LUMO level (their absolute values correspond to IP and EA, respectively, and their difference corresponds to the energy

gap). All the other levels refer also to the true quasiparticle energies, which can be directly measured by the photoemission and inverse photoemission spectroscopy. A quasiparticle wavefunction, which characterizes the electron or hole amplitude in the difference between the N-electron ground state and a $(N \pm 1)$-electron excited state, is associated with each level, and its characterization is indicated in a standard fashion as σ_g(2s) in the figure (asterisk (*) denotes an antibonding orbital, and PW denotes a plane-wave-like extended state associated with p orbitals). Note that there is a large energy gap between the occupied and unoccupied states even though their characterizations of the quasiparticle wavefunctions are the same as, e.g., π_u(2p); this situation cannot be realized within the LDA or the GGA. In the GWA, if one of the levels is occupied, a large exchange interaction separates it from the other, leading to a large energy gap.

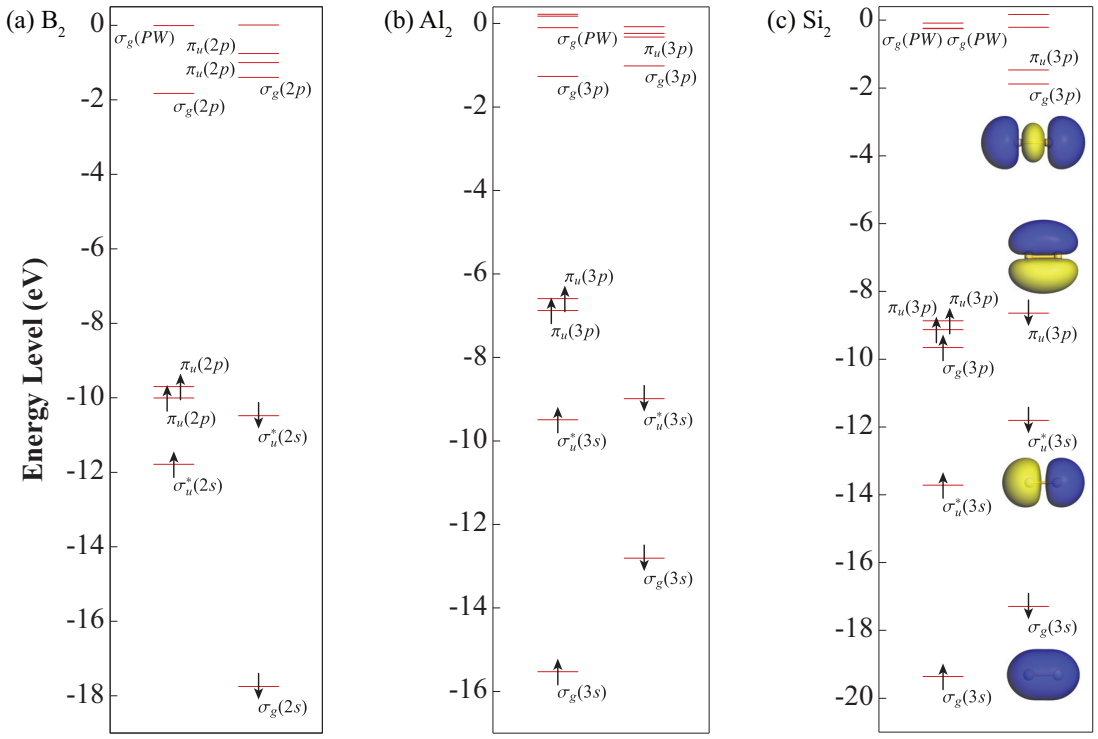

Fig.2.9: Quasiparticle energy diagrams of (a) B_2, (b) Al_2, and (c) Si_2 obtained by the GWA calculation. The quasiparticle wave functions are only drawn for Si_2, but they are similar for all the other dimers. The levels with up and down arrows (indicating electron spins) denote hole levels and those without arrows denote electron levels. The topmost level with an arrow corresponds to the HOMO level and the lowermost level without an arrow corresponds to the LUMO level; their absolute values correspond to IP and EA, respectively. Their difference corresponds to the energy gap.

Chapter 3

Linearized GW Approach Satisfying the Ward Identity: Total Energy Calculation Based on the Luttinger–Ward Functional

3.1 Introduction

The Green's function method in the many-body perturbation theory plays a powerful role in first-principles calculations of excited states of materials. The poles and residues of the one-particle Green's function G directly give the quasi-particle energy spectrum and the corresponding partial density matrix composed of a product of quasi-particle wavefunctions, respectively. Within this framework, electronic states are described by quasi-particles, and many-body interactions are represented by the self-energy Σ, which is expanded with Green's function and the Coulomb interaction v. Quasi-particles can be regarded as apparent independent particles dressed by a self-energy cloud. Almost 50 years ago, Hedin [3] proposed a closed set of equations for Green's function, the dynamically screened Coulomb interaction W (composed of the polarization function P), and the vertex function Γ. Its simplest approximation is called the GW approximation or the self-consistent GW approach, where the vertex function is replaced by unity. In this approximation, P and W become those of the random phase approximation (RPA) and the self-energy Σ is given by iGW symbolically. Furthermore, its non-self-consistent approach, which is called the one-shot GW or G_0W_0, provides a tractable scheme requiring only a moderate computational

time. This approach is justified as a first-order perturbation theory with respect to the dynamically screened Coulomb interaction W, and has been successfully applied to various solids and nano-particles, and the band gap of semiconductors and insulators as well as the ionization potential and electron affinity of atoms and molecules have been shown in good agreement with experiments [6–8].

Luttinger and Ward [14] first showed that the total energy is given by the Luttinger–Ward (LW) functional $\Phi[G]$ and some other contributions easily estimated, and the self-energy $\Sigma[G]$ is derived from a functional derivative of $\Phi[G]$ with respect to Green's function G. The important point is that it satisfies the variational principle. Using this fact, the total energy has been estimated by a robust calculation of the LW functional Φ from the one-shot GW and other approaches [15, 16, 50]. The self-consistent GW approach is identical to the shielding approximation proposed earlier by Baym and Kadanoff [4], who showed that any LW functional $\Phi[G]$ given by a restricted sum of diagrams constitutes a theory satisfying macroscopic conservation laws for the number of particles, momentum, and angular momentum, if the self-energy is given by $\Sigma[G] = \delta\Phi[G]/\delta G$. Such a theory including the shielding approximation is called the conserving approximation. It can be shown that in the conserving approximation, the virial theorem is exactly satisfied [5]. However, as a deficiency of the self-consistent GW approximation, the Ward–Takahashi identity [11], which is derived from gauge invariance, is not satisfied. Consequently, the band gap of crystals is overestimated compared with the one-shot GW. In order to satisfy the Ward–Takahashi identity, the vertex function must be included in the self-energy and the polarization function, which is a very difficult task.

Another difficulty in the quasi-particle representation is that the quasi-particle wavefunctions are non-orthonormal and linearly dependent due to the energy dependence of the self-energy. One way to solve this problem is to use Löwdin's symmetrized orthonormalization procedure, but there is a big question how to deal with this energy dependence when the quasi-particle equation is solved self-consistently.

3.2 Theory

3.2.1 Linearization

The quasiparticle equation can be written as

$$\left(\hat{T} + \hat{v}_{\mathrm{nuc}} + \Sigma(\epsilon_n)\right) | n \rangle = \epsilon_n | n \rangle, \tag{3.1}$$

where the eigenstates $| n \rangle$ are the quasiparticle states, the eigenvalues ϵ_n are the quasiparticle energies, $\hat{T}$ is the kinetic energy operator, $\hat{T} = \int | \boldsymbol{r} \rangle(-\nabla^2/2)\langle \boldsymbol{r} | d\boldsymbol{r}$, $\hat{v}_{\mathrm{nuc}}$ is the nucleus Coulomb potential, and $\Sigma(\epsilon_n)$ is the self-energy operator. Note that the self-energy operator is energy dependent, and therefore the quasiparticle states are non-orthonormal and linearly dependent. This fact makes the subsequent formulation very difficult. To avoid this difficulty, we expand the self-energy with respect to the eigenvalue ϵ_n to obtain

$$H | n \rangle = \epsilon_n \Lambda | n \rangle, \tag{3.2}$$

$$H = \hat{T} + \hat{v}_{\mathrm{nuc}} + \Sigma(\mu) - \mu \left.\frac{\partial \Sigma(\omega)}{\partial \omega}\right|_{\omega=\mu}, \tag{3.3}$$

where Λ is defined by

$$\Lambda = 1 - \left.\frac{\partial \Sigma(\omega)}{\partial \omega}\right|_{\omega=\mu}. \tag{3.4}$$

Here, μ can be set, for example, at the mean eigenvalue of the highest occupied molecular orbital (HOMO) and the lowest unoccupied molecular orbital (LUMO) levels. Although Shishkin *et al.* [12] introduced n-dependent μ and Λ, and transformed H as $\Lambda^{-1/2} H \Lambda^{-1/2}$ for each n (this is the reason why they had to introduce the matrix orthonormalization additionally), here we use n-independent μ and Λ, and the Cholesky decomposition with the lower triangular matrix L as

$$\Lambda = LL^{\dagger}. \tag{3.5}$$

Then we can naturally define the orthonormalized quasiparticle states and the corresponding Hamiltonian as

$$| \widetilde{n} \rangle = L^{\dagger} | n \rangle, \ \widetilde{H} = L^{-1} H L^{-1\dagger}. \tag{3.6}$$

As a consequence, we have the linearized quasiparticle equation:

$$\widetilde{H} | \widetilde{n} \rangle = \epsilon_n | \widetilde{n} \rangle. \tag{3.7}$$

The orthonormalized states satisfy the following orthonormality and completeness conditions:

$$\langle \widetilde{n} \mid \widetilde{m} \rangle = \delta_{nm}, \ \sum_n \mid \widetilde{n} \rangle\langle \widetilde{n} \mid \ = 1. \tag{3.8}$$

The occupation number of these states is purely zero or one according to whether the corresponding quasiparticle energy is above or below the Fermi level. In contrast, the original quasiparticle states satisfy the following equations:

$$\langle n \mid \Lambda \mid m \rangle = \delta_{nm}, \ \sum_n \mid n \rangle\langle n \mid \ = \Lambda^{-1}. \tag{3.9}$$

Since $\mid n \rangle$ do not satisfy the completeness condition, Green's function defined in this linearized framework,

$$\begin{aligned} G(\omega) &= \sum_n \frac{\mid n \rangle\langle n \mid}{\omega - \epsilon_n - i\eta_n} \\ &= \sum_n \frac{\Lambda}{(\omega - i\eta_n)\Lambda - H} \mid n \rangle\langle n \mid , \end{aligned} \tag{3.10}$$

does not have a "resolvent" form. This is because Eq.(3.10) corresponds only to the coherent part of the total Green's function (See Eq.(4-15) of Ref. [51]). In fact, this Green's function does not satisfy the charge conservation. It is readily seen from

$$-i \iint \langle \boldsymbol{r} \mid G(\omega) \mid \boldsymbol{r} \rangle d\boldsymbol{r} \frac{d\omega}{2\pi} \neq N. \tag{3.11}$$

This violation of the charge conservation is related to the existence of the incoherent part in Green's function. In order to avoid this difficulty, we introduce the renormalized Green's function as:

$$\begin{aligned} \widetilde{G}(\omega) = L^{\dagger} G(\omega) L &= \sum_n \frac{\mid \widetilde{n} \rangle\langle \widetilde{n} \mid}{\omega - \epsilon_n - i\eta_n} \\ &= \sum_n \frac{\mid \widetilde{n} \rangle\langle \widetilde{n} \mid}{\omega - i\eta_n - \widetilde{H}}. \end{aligned} \tag{3.12}$$

In this representation, since the quasiparticle states are orthonormal, Eq.(3.11) with $\widetilde{G}$ in place of G satisfies the charge conservation;

$$\int \rho(\boldsymbol{r}) d\boldsymbol{r} = -i \iint \langle \boldsymbol{r} \mid \widetilde{G}(\omega) \mid \boldsymbol{r} \rangle d\boldsymbol{r} \frac{d\omega}{2\pi} = N. \tag{3.13}$$

Note that the coherent part of the original Green's function is given by $G(\omega) = L^{-1\dagger} \widetilde{G}(\omega) L^{-1}$, and the matrices $L^{-1\dagger}$ and L^{-1} correspond to the square root of the

renormalization factor $Z = \Lambda^{-1}$ (See Eq.(4-63) of Ref. [51]). Then we should write the Hartree term as

$$\begin{aligned}\Sigma_{\mathrm{H}}(\boldsymbol{r}) &= -i \int v(\boldsymbol{r}-\boldsymbol{r}')\widetilde{G}(\boldsymbol{r},\boldsymbol{r}';\omega)d\boldsymbol{r}'\frac{d\omega}{2\pi} \\ &= \int v(\boldsymbol{r}-\boldsymbol{r}')\rho(\boldsymbol{r}')d\boldsymbol{r}', \end{aligned} \tag{3.14}$$

where $v(\boldsymbol{r}-\boldsymbol{r}')$ is the bare Coulomb interaction.

The most important fact here is that the vertex function is related to Λ via the Ward identity , i.e., the Ward–Takahashi identity in the $\boldsymbol{q} = 0$ and $\omega - \omega' = 0$ limit,

$$\Gamma(\omega = \mu, \omega' = \mu; \boldsymbol{q} = 0) = 1 - \left.\frac{\partial\Sigma(\omega)}{\partial\omega}\right|_{\omega=\mu} = \Lambda. \tag{3.15}$$

This relation can be also written as the well-known formula $\Gamma Z = 1$. The formulation up to here is very general and can be applied to any Green's function-based framework. Now, according to the Hedin's set of equations, the exact self-energy $\Sigma_{\mathrm{xc}}(\omega)$ except for the Hartree term is approximated as

$$\begin{aligned}\Sigma_{\mathrm{xc}}(\omega) &= i \int G(\omega')W(\omega-\omega')\Gamma(\omega,\omega')\frac{d\omega'}{2\pi} \\ &\approx i \int \widetilde{G}(\omega')W(\omega-\omega')\frac{d\omega'}{2\pi}, \end{aligned} \tag{3.16}$$

where we used the relation $\mathrm{Tr}[GW\Lambda] = \mathrm{Tr}[L^{\dagger}GLW] = \mathrm{Tr}[\widetilde{G}W]$. The dynamically screened Coulomb interaction W is described by the polarization function P and the interaction kernel $\delta\Sigma_{\mathrm{H}}/\delta G$ as

$$W = \left[1 - i\frac{\delta\Sigma_{\mathrm{H}}}{\delta G}P\right]^{-1} v. \tag{3.17}$$

Since the exact polarization function P is given by $P = -iGG\Gamma$ and the interaction kernel is given by

$$\frac{\delta\Sigma_{\mathrm{H}}}{\delta G} = \frac{\delta\Sigma_{\mathrm{H}}}{\delta\widetilde{G}}\frac{\delta\widetilde{G}}{\delta G} = -iv\Lambda, \tag{3.18}$$

we find that W is equal to

$$W = [1 - v\widetilde{P}]^{-1}v, \tag{3.19}$$

where we defined the renormalized polarization function as

$$\widetilde{P} = \Lambda P = -i\Lambda GG\Gamma \approx -i\Lambda GG\Lambda = -i\widetilde{G}\widetilde{G}. \tag{3.20}$$

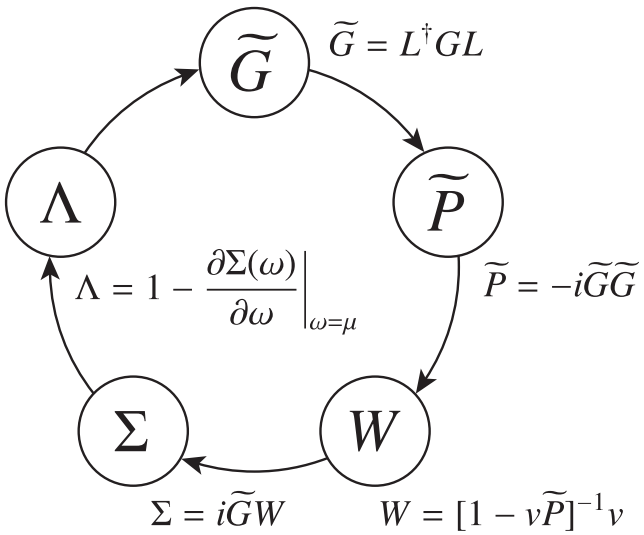

Fig.3.1: The schematic flow of the linearized self-consistent GW approach.

Therefore $\Sigma_{\rm xc}$ and W are functionals only of $\widetilde{G}$. The flow of the present computational scheme is very simple and is shown in Fig.3.1. Thus, our formulation is identical to that of the non-linearized self-consistent GW approach with G replaced by $\widetilde{G}$.

3.2.2 Total Energy

The Luttinger–Ward functional $\Phi[\widetilde{G}]$ with the renormalized Green's function $\widetilde{G}$ is given by

$$\begin{aligned}\Phi[\widetilde{G}] &= -\frac{1}{2}\lim_{\lambda\to 1}\sum_{n=1}^{\infty}\frac{\lambda^n}{n}\,\mathrm{Tr}\left\{\Sigma_n[\widetilde{G}]\,\widetilde{G}\right\} \\ &= -\frac{1}{2}\int_0^1\frac{d\lambda}{\lambda}\,\mathrm{Tr}\left\{\sum_{n=1}^{\infty}\lambda^n\Sigma_n[\widetilde{G}]\,\widetilde{G}\right\}, \end{aligned} \tag{3.21}$$

where λ is a virtual parameter corresponding to the interaction strength that becomes unity when the full Coulomb interaction is switched on, $\Sigma_n[\widetilde{G}]$ represents the contribution of the n-th order skeleton diagrams to the self-energy. This functional is diagrammatically represented by Fig.3.2. According to the general theory [51], the total energy of the ground state $E_{\rm G}^N$ with the LW functional is given by

$$E_{\rm G}^N = E_0 + \Phi[\widetilde{G}] + \mathrm{Tr}\left[\frac{\widetilde{G}}{G_0} - 1\right] - \mathrm{Tr}\left[\ln\frac{\widetilde{G}}{G_0}\right] + E_{\rm Ewald}, \tag{3.22}$$

where E_0, G_0, and E_{Ewald} are the total energy and Green's function of the non-interacting system, and the Coulombic energy between nuclei, respectively. Using the kinetic energy T and the nucleus-electron Coulomb energy $V_{\text{n-e}}$, Eq.(3.22) can be rewritten as follows:

$$E_{\text{G}}^{N} = T + V_{\text{n-e}} + \Phi[\widetilde{G}] + E_{\text{Ewald}}, \tag{3.23}$$

where T and $V_{\text{n-e}}$ are given by

$$\begin{aligned} T &= -i \int \left[\lim_{\boldsymbol{r}\to\boldsymbol{r}'} \left(-\frac{1}{2}\nabla^2 \right) \langle\, \boldsymbol{r} \,|\, \widetilde{G}(\omega) \,|\, \boldsymbol{r}' \,\rangle \right] d\boldsymbol{r} \frac{d\omega}{2\pi} \\ &= \sum_{n}^{\text{occ}} \int \langle\, \widetilde{n} \,|\, \boldsymbol{r} \,\rangle \left(-\frac{1}{2}\nabla^2 \right) \langle\, \boldsymbol{r} \,|\, \widetilde{n} \,\rangle d\boldsymbol{r}, \end{aligned} \tag{3.24}$$

$$V_{\text{n-e}} = \sum_{n}^{\text{occ}} \langle\, \widetilde{n} \,|\, \hat{v}_{\text{nuc}} \,|\, \widetilde{n} \,\rangle. \tag{3.25}$$

The Hartree and exchange part of the LW functional (Φ_{H} and Φ_{x}) are λ-independent, and they can be evaluated as

$$\begin{aligned} \Phi_{\text{A}}[\widetilde{G}] = V_{\text{A}} &= -\frac{i}{2} \int \langle\, \boldsymbol{r} \,|\, \Sigma_{\text{A}} \widetilde{G}(\omega) \,|\, \boldsymbol{r} \,\rangle d\boldsymbol{r} \frac{d\omega}{2\pi} \\ &= \frac{1}{2} \sum_{n}^{\text{occ}} \langle\, \widetilde{n} \,|\, \Sigma_{\text{A}} \,|\, \widetilde{n} \,\rangle, \qquad (\text{A} = \text{H or x}), \end{aligned} \tag{3.26}$$

where V_{H} and V_{x} are the Hartree and exchange energy. In the next subsection, we present a convenient formula to calculate the correlation part of LW functional $\Phi_{\text{c}}[\widetilde{G}]$ within a plasmon-pole model.

3.2.3 LW Functional

As shown in Fig.3.2, $\Phi[\widetilde{G}]$ is a sum of the skeleton diagrams, which corresponds to the sum of the ring diagrams in the random phase approximation (RPA) made up of $\widetilde{G}$. In the case of the non-linearized self-consistent GW or the one-shot GW method, $\widetilde{G}$ can be replaced by G or G_0. (G_0 is obtained from local density approximation (LDA) or Hartree–Fock (HF) calculations.) In any case, the parameter λ appears as a prefactor for the RPA polarization part that diagrammatically corresponds to a ring. Our idea is to use the von der Linden and Horsch (vdLH) plasmon-pole model [25], and to solve the λ-independent eigenvalue problem of the symmetrized Hermitian

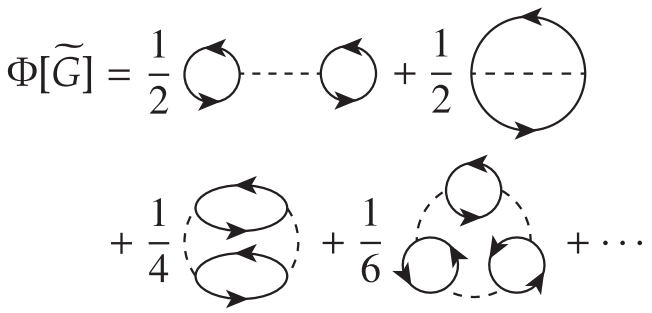

Fig.3.2: The Feynman diagram of the Luttinger–Ward functional within the LGW approximation. The solid line and dashed line are the renormalized Green's function and the bare Coulomb interaction, respectively.

product of the Coulomb interaction $v(\boldsymbol{G}) = 4\pi/\Omega\boldsymbol{G}^2$ (Ω is the volume of the unit cell) and the RPA polarization part

$$v(\boldsymbol{G}) \sum_{\boldsymbol{G}'} \frac{|\boldsymbol{G}|}{|\boldsymbol{G}'|} P_{\boldsymbol{G}\boldsymbol{G}'}(\omega = 0) u_p(\boldsymbol{G}') = \chi_p u_p(\boldsymbol{G}), \tag{3.27}$$

instead of solving the original λ-dependent eigenvalue problem of the *inverse* symmetrized dielectric matrix. The eigenvalue χ_p is related to the plasmon strength $z_p(\lambda)$ via

$$\frac{1}{1 - \lambda\chi_p} = \lim_{\omega \to 0} \left[1 + \frac{z_p(\lambda)\omega_p^2(\lambda)}{\omega^2 - (\omega_p(\lambda) - i\eta)^2} \right] = 1 - z_p(\lambda), \tag{3.28}$$

where η is a positive infinitesimal. The plasmon-pole frequency $\omega_p(\lambda)$ is given by the relation

$$\omega_p^2(\lambda) = \frac{4\pi\lambda}{z_p(\lambda)} \sum_{\boldsymbol{G},\boldsymbol{G}'} \Theta_p(\boldsymbol{G}) L_{\boldsymbol{G}\boldsymbol{G}'} \Theta_p(\boldsymbol{G}') \equiv \frac{\lambda\alpha^2}{z_p(\lambda)}, \tag{3.29}$$

where we put $L_{\boldsymbol{G}\boldsymbol{G}'} = \boldsymbol{G} \cdot \boldsymbol{G}' n(\boldsymbol{G}')$ and $\Theta_p(\boldsymbol{G}) = u_p(\boldsymbol{G})/|\boldsymbol{G}|$. Therefore, we have $z_p(\lambda) = \lambda/(\lambda - \chi_p^{-1})$ and $\omega_p^2(\lambda) = \alpha^2(\lambda - \chi_p^{-1})$. Using the λ-dependent formulae above for the vdLH plasmon-pole model, the correlation part of the LW functional, $\Phi_c[\widetilde{G}]$, is given by

$$\Phi_c[\widetilde{G}] = -\frac{2\pi i}{\Omega} \sum_n \sum_m \sum_p \frac{1}{2} \int_0^1 \frac{d\lambda}{\lambda} \int_{-\infty}^{\infty} \frac{d\omega}{2\pi} \frac{1}{\omega - \epsilon_n - i\eta_n} \times \frac{\lambda z_p(\lambda)\omega_p(\lambda)[M_p^{m\,n}]^* M_p^{m\,n}}{\omega - \epsilon_m + \omega_p(\lambda)\mathrm{sgn}(\mu - \epsilon_m) - i\eta_m}$$

$$= \frac{2\pi}{\Omega}\sum_{n}^{\mathrm{occ}}\sum_{m}^{\mathrm{emp}}\sum_{p}\frac{1}{2}\int_0^1 d\lambda \frac{z_p(\lambda)\omega_p(\lambda)[M_p^{m\,n}]^* M_p^{m\,n}}{\epsilon_n - \epsilon_m + \omega_p(\lambda)\mathrm{sgn}(\mu-\epsilon_m) + i\eta}$$
$$- \frac{2\pi}{\Omega}\sum_{n}^{\mathrm{emp}}\sum_{m}^{\mathrm{occ}}\sum_{p}\frac{1}{2}\int_0^1 d\lambda \frac{z_p(\lambda)\omega_p(\lambda)[M_p^{m\,n}]^* M_p^{m\,n}}{\epsilon_n - \epsilon_m + \omega_p(\lambda)\mathrm{sgn}(\mu-\epsilon_m) - i\eta} \tag{3.30}$$

where we put

$$M_p^{m\,n} = \sum_{\boldsymbol{G}} \langle\, \widetilde{m}\,|\, e^{-i\boldsymbol{G}\cdot\boldsymbol{r}}\,|\,\widetilde{n}\,\rangle \Theta_p^*(\boldsymbol{G}). \tag{3.31}$$

Here we present the detailed procedure of the λ integral in Eq.(3.30). The λ-dependent part in Eq.(3.30) is given by

$$I = \frac{1}{2}\int_0^1 d\lambda \frac{z_p(\lambda)\omega_p(\lambda)}{\epsilon_n - \epsilon_m \pm \omega_p(\lambda)}. \tag{3.32}$$

Here, we put $s = (\epsilon_n - \epsilon_m)/\alpha$ (α is the λ-independent constant defined in Eq.(2.19)) and $\xi = \sqrt{\lambda - \chi_p^{-1}}$. The integration above is then evaluated as

$$\begin{aligned} I &= \frac{1}{2}\int_{\xi_0}^{\xi_1} \frac{\xi^2 + \chi_p^{-1}}{\xi(s\pm\xi)} 2\xi d\xi \\ &= \int_{\xi_0}^{\xi_1} \frac{-(s-\xi)(s+\xi) + s^2 + \chi_p^{-1}}{s\pm\xi} d\xi \\ &= \int_{\xi_0}^{\xi_1} \left[-(s\mp\xi) + \frac{s^2+\chi_p^{-1}}{s\pm\xi}\right] d\xi \\ &= -s(\xi_1 - \xi_0) \pm \frac{1}{2} \pm \left(s^2 + \chi_p^{-1}\right)\log\left|\frac{s\pm\xi_1}{s\pm\xi_0}\right|, \end{aligned} \tag{3.33}$$

where $\xi_0 = \sqrt{-\chi_p^{-1}}$ and $\xi_1 = \sqrt{1-\chi_p^{-1}}$. Alternatively, if we ignore the λ-dependence in $\omega_p(\lambda)$, Eq.(3.32) can be evaluated as

$$\begin{aligned} I &= \frac{1}{2}\int_0^1 d\lambda \frac{z_p(\lambda)\omega_p}{\epsilon_n - \epsilon_m \pm \omega_p} \\ &= \frac{1}{2}\left(1 + \chi_p^{-1}\log|1-\chi_p|\right)\frac{\omega_p}{\epsilon_n - \epsilon_m \pm \omega_p}. \end{aligned} \tag{3.34}$$

We checked that the correlation energies with these two formulae do not differ significantly. An advantage of using Eq.(3.34) is that the projection operator can be used

to evaluate the λ-independent part of the Luttinger–Ward functional as follows:

$$
\begin{aligned}
\Phi_{\rm c}[\widetilde{G}] = & \frac{2\pi}{\Omega}\sum_{p}\sum_{n}^{\rm occ}\sum_{m}^{\rm emp}\frac{1}{2}\frac{\omega_p\left(1+\chi_p^{-1}\log|1-\chi_p|\right)M_p^{m\,n}[M_p^{m\,n}]^*}{\epsilon_n-\epsilon_m+\omega_p{\rm sgn}(\mu-\epsilon_{\rm m})+i\eta} \\
& -\frac{2\pi}{\Omega}\sum_{p}\sum_{n}^{\rm emp}\sum_{m}^{\rm occ}\frac{1}{2}\frac{\omega_p\left(1+\chi_p^{-1}\log|1-\chi_p|\right)M_p^{m\,n}[M_p^{m\,n}]^*}{\epsilon_n-\epsilon_m+\omega_p{\rm sgn}(\mu-\epsilon_{\rm m})-i\eta} \\
= & \frac{\pi}{\Omega}\sum_{p}\sum_{n}^{\rm occ}\omega_p\left(1+\chi_p^{-1}\log|1-\chi_p|\right) \\
& \times\sum_{\boldsymbol{G}}\Theta_p(\boldsymbol{G})\langle\,\widetilde{n}\,|\,e^{i\boldsymbol{G}\cdot\boldsymbol{r}}\frac{\hat{P}}{\epsilon_n-\omega_p+i\eta-\widetilde{H}}\sum_{\boldsymbol{G}'}e^{-i\boldsymbol{G}'\cdot\boldsymbol{r}'}\,|\,\widetilde{n}\,\rangle\Theta_p^*(\boldsymbol{G}') \\
& +\frac{\pi}{\Omega}\sum_{p}\sum_{n}^{\rm occ}\omega_p\left(1+\chi_p^{-1}\log|1-\chi_p|\right) \\
& \times\sum_{\boldsymbol{G}'}\Theta_p^*(\boldsymbol{G}')\langle\,\widetilde{n}\,|\,e^{-i\boldsymbol{G}'\cdot\boldsymbol{r}'}\frac{\hat{P}}{\epsilon_n-\omega_p+i\eta-\widetilde{H}}\sum_{\boldsymbol{G}}e^{i\boldsymbol{G}\cdot\boldsymbol{r}}\,|\,\widetilde{n}\,\rangle\Theta_p(\boldsymbol{G}) \qquad (3.35)
\end{aligned}
$$

We also checked that the empty levels taken into account for the summation in Eq.(3.30) is good enough if it is taken up to about 1500 levels.

3.2.4 Projection Operator

We introduce the projection operator to save a computational time for the evaluation of Eqs.(3.16) and (3.20), in which the summation over infinite unoccupied states can be exactly projected onto the subspace of only occupied states. The projection operator $\hat{P}$ is defined as

$$
\hat{P}=\sum_{n}^{\rm emp}|\,\widetilde{n}\,\rangle\langle\,\widetilde{n}\,|\;=1-\sum_{n}^{\rm occ}|\,\widetilde{n}\,\rangle\langle\,\widetilde{n}\,|\,. \qquad (3.36)
$$

In practice, the quasiparticle states are expanded in terms of a basis set $|\,\alpha\,)$ as

$$
|\,n\,\rangle=\sum_{\alpha}c_{n\,\alpha}\,|\,\alpha\,). \qquad (3.37)
$$

In general, the basis functions are non-orthogonal to each other, and we define the overlap matrix as $S_{\alpha\,\beta}=(\,\alpha\,|\,\beta\,)$. The quasiparticle equation Eq.(3.2) with Eq.(3.3) can

be rewritten in this representation as the following generalized eigenvalue problem:

$$\sum_{\beta}(\,\alpha\,|\left[\hat{T}+\hat{v}_{\mathrm{nuc}}+\Sigma(\mu)-\mu\frac{\partial\Sigma(\omega)}{\partial\omega}\Big|_{\omega=\mu}\right]|\,\beta\,)c_{n\beta}$$
$$=\epsilon_n\sum_{\beta}(\,\alpha\,|\,\Lambda\,|\,\beta\,)c_{n\beta}. \tag{3.38}$$

Consequently, the exchange and correlation terms of the self-energy ($\Sigma_{\mathrm{xc}}(\omega)=\Sigma_{\mathrm{x}}+\Sigma_{\mathrm{c}}(\omega)$) and the renormalized polarization function can be evaluated as

$$(\,\alpha\,|\,\Sigma_{\mathrm{x}}\,|\,\beta\,)=-\frac{4\pi}{\Omega}\sum_{\boldsymbol{G}}\sum_{n}^{\mathrm{occ}}\frac{(\,\alpha\,|\,e^{i\boldsymbol{G}\cdot\boldsymbol{r}}\,|\,\widetilde{n}\,\rangle\langle\,\widetilde{n}\,|\,e^{-i\boldsymbol{G}\cdot\boldsymbol{r}'}\,|\,\beta\,)}{\boldsymbol{G}^2}, \tag{3.39}$$

$$(\,\alpha\,|\,\Sigma_{\mathrm{c}}(\mu)\,|\,\beta\,)=\frac{2\pi}{\Omega}\sum_{p}\sum_{n}^{\mathrm{occ}}z_p\omega_p[\Xi_p^{n\,\alpha}]^*\frac{1}{\mu+\omega_p-\epsilon_n-i\eta}\Xi_p^{n\,\beta}$$
$$+\frac{2\pi}{\Omega}\sum_{p}z_p\omega_p[\Pi_p^{\alpha}]^{\dagger}\frac{\hat{P}}{\mu-\omega_p+i\eta-\widetilde{H}}\Pi_p^{\beta}, \tag{3.40}$$

$$\widetilde{P}_{\boldsymbol{G}\,\boldsymbol{G}'}(\omega)=\sum_{n}^{\mathrm{occ}}\langle\,\widetilde{n}\,|\,e^{-i\boldsymbol{G}\cdot\boldsymbol{r}}\frac{\hat{P}}{\epsilon_n+i\eta-\omega-\widetilde{H}}e^{i\boldsymbol{G}'\cdot\boldsymbol{r}'}\,|\,\widetilde{n}\,\rangle$$
$$+\sum_{n}^{\mathrm{occ}}\langle\,\widetilde{n}\,|\,e^{i\boldsymbol{G}'\cdot\boldsymbol{r}'}\frac{\hat{P}}{\epsilon_n+i\eta+\omega-\widetilde{H}}e^{-i\boldsymbol{G}\cdot\boldsymbol{r}}\,|\,\widetilde{n}\,\rangle, \tag{3.41}$$

where we put

$$\Xi_p^{n\,\beta}=\sum_{\boldsymbol{G}}\langle\,\widetilde{n}\,|\,e^{-i\boldsymbol{G}\cdot\boldsymbol{r}}\,|\,\beta\,)\Theta_p^*(\boldsymbol{G}), \tag{3.42}$$

$$\Pi_p^{\beta}=\sum_{\boldsymbol{G}}e^{-i\boldsymbol{G}\cdot\boldsymbol{r}}\,|\,\beta\,)\Theta_p^*(\boldsymbol{G}). \tag{3.43}$$

Here, $\omega_p=\omega_p(\lambda=1)$, $z_p=z_p(\lambda=1)$, and $\Theta_p(\boldsymbol{G})$ are the plasmon-pole frequency, strength, and the scaled plasmon-pole eigenvector, respectively, as defined in the previous subsection. The summation over the plasmon-pole frequency ω_p in Eq.(3.40) should be taken afterwards. The number of ω_p's is equal to the number of $\boldsymbol{G}$'s, and is quite large. However, it is generally enough to preserve only about a first hundred of the plasmon-pole frequencies in ascending order.

3.3 Methodology

We chose simple isolated Li and Na systems (atoms and dimers) to validate our approach, because clusters composed of more than two atoms have an ambiguity of

their shape, but dimer does not have such an ambiguity. For Li and Na atoms, we performed the spin-dependent calculation.

We used the all-electron mixed basis approach, where the one particle wave functions are expanded with the combination of plane waves and atomic orbitals. This approach can describe both deep core states and plane-wave-like continuous states efficiently and appropriately compared to the approaches which use only plane waves or only localized orbitals as basis functions.

The spherical cut technique is used to ignore the interaction with the periodic images. The atoms and dimers are put in the rhombohedral unit cell with $a = b = c = 16$ Å and $\alpha = \beta = \gamma = 60°$. We checked that the total energy, the ionization potential, and the electron affinity are enough converged with respect to the unit cell size. The cutoff energy $E_{\rm cut}$ for the plane waves and $\boldsymbol{G}$, $\boldsymbol{G}'$ in Eq.(3.41) as well as the cutoff energy $E^{\rm x}_{\rm cut}$ of $\boldsymbol{G}$ in Eq.(3.39) are carefully determined by convergence tests. $E_{\rm cut}$ and $E^{\rm x}_{\rm cut}$ are 71 and 339 eV, respectively.

We used the numerical differentiation around $\mu = (\epsilon_{\rm HOMO} + \epsilon_{\rm LUMO})/2$:

$$\left.\frac{\partial\Sigma(\omega)}{\partial\omega}\right|_{\omega=\mu} = \frac{\Sigma(\mu+\Delta/2) - \Sigma(\mu-\Delta/2)}{\Delta} \tag{3.44}$$

with $\Delta = 0.1$ eV. We also confirmed that the self-energy does not significantly depend on the choice of μ. We first obtained the well converged electronic states within LDA, and then proceeded to the GW and LGW calculations. The criterion of the SCF convergence of LDA, HF, GW, and LGW is 10^{-6} eV in the total energy.

For the calculations with the hybrid functional B3LYP, we used the all-electron localized numerical basis program, DMol^3 [31, 32] in Materials Studio.

3.4 Results and Discussion

The results for the ionization potential (IP), which is equal to $-\epsilon_{\rm HOMO}$, and the electron affinity (EA), which is equal to $-\epsilon_{\rm LUMO}$, of Li, Li_2, Na, and Na_2 calculated with LDA, HF, the self-consistent GW (GW), and the linearized self-consistent GW (LGW) are summarized in Tables.3.1 (for Li and Li_2) and 3.2 (for Na and Na_2) together with experimental data [52–57] in units of eV.

LDA and B3LYP results of IP and EA are just the absolute values of the eigenvalues of HOMO and LUMO as well as HF, GW, and LGW. For both atoms and dimers, LDA and B3LYP give significantly large EA, and HF gives significantly small EA. In contrast, GW and LGW improve these results of EA, and LGW gives the best agree-

Table.3.1: Ionization potentials (IP) and electron affinities (EA) in eV of Li and Li_2.

	Li		Li_2	
	IP	EA	IP	EA
LDA	3.14	1.83	3.24	1.84
HF	5.34	0.04	4.88	0.08
B3LYP	3.34	1.00	3.30	0.99
GW	5.78	0.22	5.56	0.20
LGW	5.66	0.28	5.32	0.35
Expt.	5.39[a]	0.62[b]	5.15[a]	0.44[c]

[a] See Ref. [52].
[b] See Ref. [53].
[c] See Ref. [54].

Table.3.2: Ionization potentials (IP) and electron affinities (EA) in eV of Na and Na_2.

	Na		Na_2	
	IP	EA	IP	EA
LDA	3.08	2.04	3.27	1.97
HF	4.94	0.14	4.53	0.01
B3LYP	3.16	1.09	3.19	1.01
GW	5.32	0.25	5.11	0.32
LGW	5.20	0.31	4.92	0.45
Expt.	5.14[a]	0.55[b]	4.93[a]	0.43[c]

[a] See Ref. [55].
[b] See Ref. [56].
[c] See Ref. [57].

ment with the experimental data. For IP, on the other hand, LDA and B3LYP give significantly small values, while HF, GW, and LGW give reasonable values. For Li_2 and Na_2, LGW gives the best IP if we compare with the experimental data (For Li, HF accidentally gives the best IP and LGW gives the second best IP). From these tables, we find also that the energy gap, i.e., IP − EA, of GW overestimates the experimental energy gap. This is an inherent tendency of GW although there are some exceptions

such as a Ca atom [21]. That of LGW improves this inherent tendency of GW and gives smaller energy gap, which is in fairly good agreement with the experimental energy gap. Therefore, among these methods, we can conclude that LGW gives the best results comparable to the experimental IP and EA.

The absolute values of the total energy E_{G}^{N} in atomic units (a.u.) (1 a.u. = 27.2 eV) of Li, Li_2, Na, and Na_2 (at the equilibrium distance for dimers) are shown in Table.3.3 together with virial ratio $-V/T$ and components contributing to the total energy.

Table.3.3: Total energies (E_{G}^{N}), their components in units of a.u. (1 a.u. = 27.2 eV), and virial ratios ($-V/T$) calculated by various approaches. The components, T, $V_{\text{n-e}}$, V_{H}, V_{x}, E_{xc}, and Φ_{c} are the kinetic energy, the nucleus-electron Coulomb energy, Hartree energy, the Fock exchange energy, the LDA exchange-correlation energy, and the correlation energy, respectively.

		E_{G}^{N}	T	$V_{\text{n-e}}$	V_{H}	V_{x} (E_{xc})	Φ_{c}	$-V/T$
Li	LDA	−7.3430	7.3457	−16.8770	4.0287	−1.6640		1.999
	HF	−7.4327	7.4362	−17.1480	4.0588	−1.7798		2.000
	GW	−7.4419	7.4382	−17.1556	4.0660	−1.7812	−0.0092	2.000
	LGW	−7.4422	7.4675	−17.1895	4.0750	−1.7856	−0.0097	1.996
Li_2	LDA	−14.7257	14.7431	−36.1165	9.1904	−3.3625		2.000
	HF	−14.8723	14.8715	−36.3637	9.2002	−3.5539		2.000
	GW	−14.9042	14.8819	−36.4281	9.2390	−3.5537	−0.0322	2.001
	LGW	−14.9065	14.9593	−36.5180	9.2643	−3.5691	−0.0348	1.996
Na	LDA	−161.4453	161.4426	−388.6022	79.7772	−13.5275		2.000
	HF	−161.8534	161.5687	−389.5288	80.1072	−13.9948		2.002
	GW	−161.8614	161.5600	−389.5304	80.1111	−13.9941	−0.0080	2.002
	LGW	−161.8616	161.6364	−389.6607	80.1743	−14.0033	−0.0084	2.001
Na_2	LDA	−322.9698	322.9278	−775.5762	163.8824	−27.0807		2.000
	HF	−323.7526	323.1599	−777.7621	164.3155	−27.9801		2.002
	GW	−323.7805	323.1348	−777.7282	164.3387	−27.9772	−0.0281	2.002
	LGW	−323.7823	323.3651	−787.4844	164.5276	−28.0055	−0.0304	2.001

Here, E_{xc} is the exchange-correlation energy of LDA. Note that T and V in LDA are not the Kohn–Sham kinetic energy T_s and the potential energy involving E_{xc} as the exchange-correlation energy, but those estimated as $T_{\mathrm{s}} + T_{\mathrm{xc}}$ and $V_{\text{n-e}} + V_{\mathrm{H}} + E_{\mathrm{xc}} - T_{\mathrm{xc}}$ with T_{xc} given by Averill and Painter [20] who showed the validity of virial theorem in LDA. For GW and LGW, the Luttinger–Ward functional Φ_{c} is evaluated with Eq.(3.30). The correlation energy, i.e., the total energy difference between HF and GW/LGW is almost the same as the value of Φ_{c}. The resulting virial ratio is fairly good agreement with the exact value 2 in all cases. Concerning the ground-state to-

tal energy E_G^N, LGW is the deepest and GW is the second deepest, suggesting that LGW gives the best result for the correlation energy among these approximations in a sense of the variational principle. This fact can also be directly seen from the value of the Luttinger–Ward functional Φ_c in Table.3.3.

The total energy of the ground state measured from the dissociation limit is depicted versus the interatomic distance of Li_2 in units of eV in Fig.3.3. The equilibrium distances and the binding energies are different among LDA, HF, B3LYP, GW, and LGW. The bond force constant κ can be calculated from a quadratic function ($\Delta E = \kappa(\Delta d)^2/2$) fitted to the total energy curve. The equilibrium distances, the binding energies, the bond force constants, and the corresponding vibrational frequencies of Li_2 calculated with LDA, HF, B3LYP, GW, and LGW are summarized in Table.3.4.

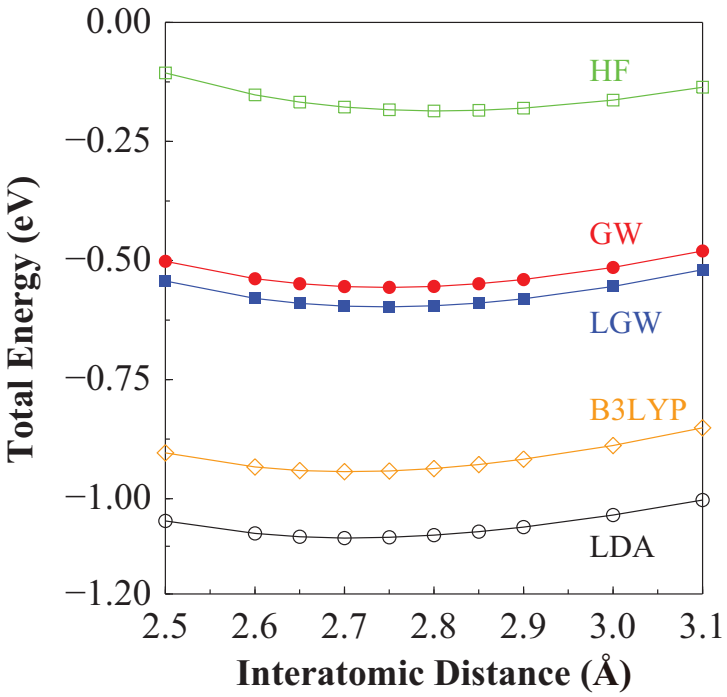

Fig.3.3: Total energies measured from the dissociation limit of Li_2 in eV as a function of the interatomic distance.

For the equilibrium distance, HF significantly overestimates the experimental value, and LDA and B3LYP are the best agreement with the experimental value. GW and LGW give the same value within the estimation error, which is intermediate between the values of LDA (B3LYP) and HF as expected. For the binding energy, HF significantly underestimates the experimental value, and LDA and B3LYP show good agreement with the experimental value. Again the GW and LGW results

Table.3.4: Equilibrium interatomic distances (d_0) in Å , binding energies (E_{bin}) in eV, bond force constants (κ) in eV/Å^2, and corresponding vibrational frequencies (f) in cm^{-1} of Li_2.

	d_0	E_{bin}	κ	f
LDA	2.70	1.08	1.47	340
HF	2.81	0.19	1.40	332
B3LYP	2.70	0.94	1.53	346
GW	2.74	0.56	1.40	331
LGW	2.74	0.60	1.41	332
Expt.	2.67[a]	1.04[a]	–	351[a]

[a] See Ref. [58].

are intermediate between the LDA (B3LYP) and HF results. The binding energy of LGW is improved than that of GW, although these values are smaller than the experimental value. For the bond force constant and the vibrational frequency, LDA gives the smallest value, HF gives the largest value, and HF, GW, and LGW give almost the same value, although the GW and LGW results are only very slightly lower than the HF result.

For the bond force constant and the vibrational frequency, HF, GW, and LGW give almost the same value, while LDA and B3LYP give slightly larger values than this value. (B3LYP is the best agreement with the experimental value among all.) All these values are, however, somewhat smaller than the experimental value. One reason of the underestimation of the binding energy and the vibrational frequency may be due to the vibrational and rotational contributions to the total free energy at finite temperatures, although we have not considered such effects because they are beyond the scope of this thesis. Another reason may be due to the missing contribution to the total energy in short wave length scales in the GW and LGW approximations. To improve GW and LGW, it is necessary to take into account the vertex correction Γ with $\boldsymbol{q} \neq 0$ and $\omega \neq \omega'$, which is not included in the present formulation. However, since the GW and LGW approximations take into account correctly the long wave length contributions within the RPA, we expect that they will reproduce correctly the long distance behaviour in a van der Waals regime.

Chapter 4

GWΓ with the All-Electron Mixed Basis Approach

4.1 Introduction

As stated in the previous chapters, the GW approximation does not include the vertex correction. As a consequence of that, the calculated ionization potentials and electron affinities for molecules and clusters within GW are generally overestimated and underestimated compared with experimental data. There are some papers to study the vertex effect for the dynamically screened interaction [12, 13]. However, the important defect of these approaches is that the Ward–Takahashi identity is not satisfied, and it is very important to include the explicit vertex function in not only the self-energy but also the polarization function. We introduce the first-order vertex correction to both the self-energy and the polarization function, and show that the our GWΓ approach satisfies the Ward–Takahashi identity within the first-order approximation for the vertex function.

4.2 Theory

In the GWΓ approach, the three-points vertex function $\Gamma(x_1, x_2; x')$ represented in Fig.4.1 is included in the polarization function and the self-energy. Here, x is defined as the space coordinates and time: $x = (\boldsymbol{r}, t)$. If we consider the first-order diagram in Fig.4.1 and replace the dynamically screened interaction W with the bare Coulomb interaction v, then the lowest order contribution of the vertex correction to

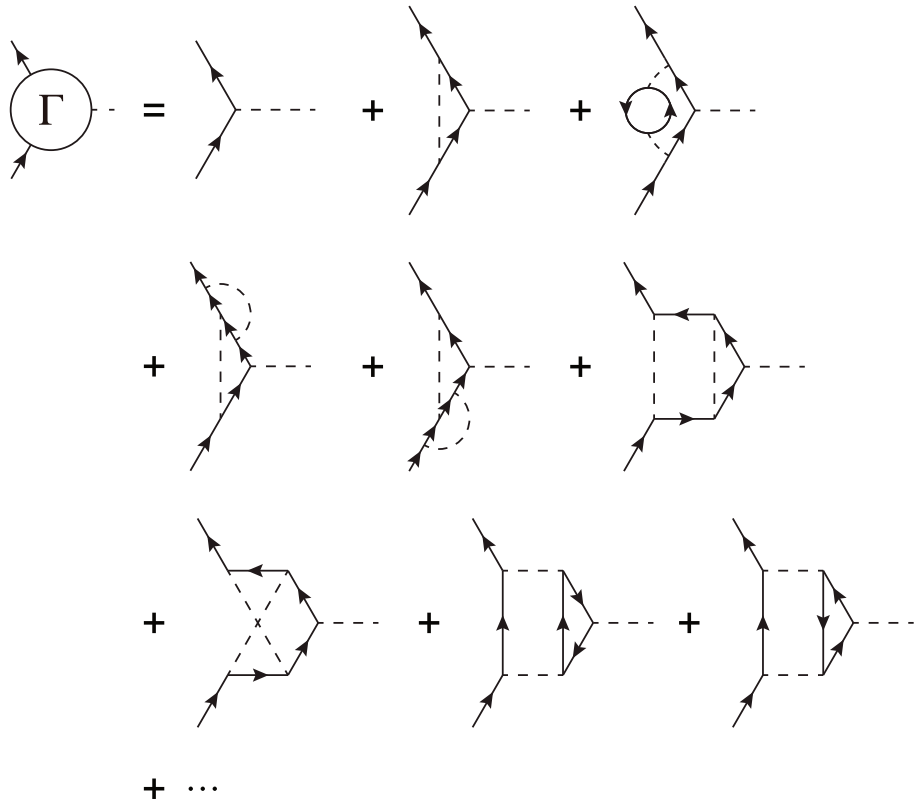

Fig.4.1: The Feynman diagrams of the vertex function. The solid and dashed lines show Green's function and the bare Coulomb interaction, respectively.

the Hartree–Fock self-energy is given by

$$\begin{aligned}\Sigma_{GV\Gamma}(x,x') &= i^2 \iint G(x,x_1)v(x-x_2)\Gamma(x_1,x_2;x')dx_1dx_2 \\ &= i^2 \iint G(x,x_1)v(x-x_2)G(x_1,x_2)v(x_1-x')G(x_2,x')dx_1dx_2, \qquad (4.1)\end{aligned}$$

and it can be diagrammatically given as shown in Fig.4.2. The Fourier transform of Eq.(4.1) is given by

$$\begin{aligned}\Sigma_{GV\Gamma}(\boldsymbol{r},\boldsymbol{r}',\omega) &= i^2 \iint G(\boldsymbol{r},\boldsymbol{r}_1,\omega-\omega')v(\boldsymbol{r}-\boldsymbol{r}_2) \\ &\qquad \Gamma(\boldsymbol{r}_1,\boldsymbol{r}_2,\boldsymbol{r}',\omega,\omega')d\omega' d\boldsymbol{r}_1 d\boldsymbol{r}_2 \\ &= i^2 \iint G(\boldsymbol{r},\boldsymbol{r}_1,\omega-\omega')v(\boldsymbol{r}-\boldsymbol{r}_2)G(\boldsymbol{r}_1,\boldsymbol{r}_2,\omega-\omega'') \\ &\qquad \times v(\boldsymbol{r}_1-\boldsymbol{r}')G(\boldsymbol{r}_2,\boldsymbol{r}',\omega-\omega'')d\omega' d\omega'' d\boldsymbol{r}_1 d\boldsymbol{r}_2. \qquad (4.2)\end{aligned}$$

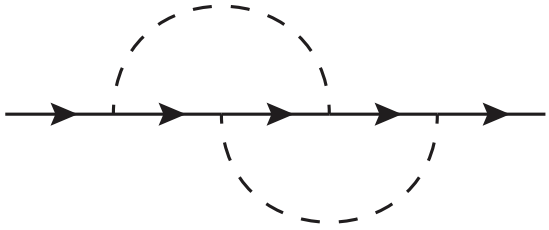

Fig.4.2: The Feynman diagrams of the second-order exchange. The solid and dashed lines show Green's function and the bare Coulomb interaction, respectively.

This diagram is the second-order exchange diagram in the Møller-Plesset perturbation theory (MP2). The second-order direct diagram is already included in the GW self-energy. The MP2 can well describe the short- or middle-range correlation, while the GW well describes the long-range correlation. Thus, adding this diagram to the GW self-energy should improve the description of the electron correlation within the GW at any range. The Eq.(4.2) can be written with the matrix representation as follows.

$$
\begin{aligned}
(\nu|\Sigma_{GV\Gamma}(\omega)|\mu) = \frac{i^2}{\Omega}\sum_{i,j,k}\sum_{\boldsymbol{G},\boldsymbol{G}'}\iint\frac{d\omega'}{2\pi}\frac{d\omega''}{2\pi} \\
\times\frac{(\nu|e^{i\boldsymbol{G}\cdot\boldsymbol{r}}|i\rangle\langle i|e^{i\boldsymbol{G}'\cdot\boldsymbol{r}''}|j\rangle\langle j|e^{-i\boldsymbol{G}\cdot\boldsymbol{r}'''}|k\rangle\langle k|e^{-i\boldsymbol{G}'\cdot\boldsymbol{r}'}|\mu)}{\omega-\omega'-(\epsilon_i+i\eta_i)} \\
\times\frac{v(\boldsymbol{G})v(\boldsymbol{G}')}{(\omega-\omega'-\omega''-(\epsilon_j+i\eta_j))(\omega-\omega''-(\epsilon_k+i\eta_k))} \\
=\frac{1}{\Omega}\sum_{\boldsymbol{G},\boldsymbol{G}'}(\nu|e^{i\boldsymbol{G}\cdot\boldsymbol{r}}|i\rangle\langle i|e^{i\boldsymbol{G}'\cdot\boldsymbol{r}''}|j\rangle\langle j|e^{-i\boldsymbol{G}\cdot\boldsymbol{r}'''}|k\rangle\langle k|e^{-i\boldsymbol{G}'\cdot\boldsymbol{r}'}|\mu) \\
\times\Bigg(\sum_i^{\mathrm{occ}}\sum_j^{\mathrm{emp}}\sum_k^{\mathrm{occ}}\frac{1}{\epsilon_i-\epsilon_j+\epsilon_k-\omega+i\eta} \\
+\sum_i^{\mathrm{emp}}\sum_j^{\mathrm{occ}}\sum_k^{\mathrm{emp}}\frac{1}{\epsilon_i-\epsilon_j+\epsilon_k-\omega-i\eta}\Bigg)v(\boldsymbol{G})v(\boldsymbol{G}') \qquad (4.3)
\end{aligned}
$$

In the same manner as the second-exchange term, the second-order direct term (diagrammatically shown in Fig.4.3) can be given by

$$
\begin{aligned}
(\nu|\Sigma_{\text{2nd Direct}}(\omega)|\mu) = -\frac{i^2}{\Omega}\sum_{i,j,k}\sum_{\boldsymbol{G},\boldsymbol{G}'}\iint\frac{d\omega'}{2\pi}\frac{d\omega''}{2\pi} \\
\frac{(\nu|e^{i\boldsymbol{G}\cdot\boldsymbol{r}}|i\rangle\langle j|e^{-i\boldsymbol{G}\cdot\boldsymbol{r}''}|k\rangle\langle k|e^{i\boldsymbol{G}'\cdot\boldsymbol{r}'''}|j\rangle\langle i|e^{-i\boldsymbol{G}'\cdot\boldsymbol{r}'}|\mu)}{\omega-\omega'-(\epsilon_i+i\eta_i)}
\end{aligned}
$$

$$\times \frac{v(\boldsymbol{G})v(\boldsymbol{G}')}{(\omega'' - (\epsilon_j + i\eta_j))(\omega'' + \omega' - (\epsilon_k + i\eta_k))}$$

$$= -\frac{1}{\Omega}\sum_{\boldsymbol{G},\boldsymbol{G}'}(v|e^{i\boldsymbol{G}\cdot\boldsymbol{r}}|i\rangle\langle j|e^{-i\boldsymbol{G}\cdot\boldsymbol{r}''}|k\rangle\langle k|e^{i\boldsymbol{G}'\cdot\boldsymbol{r}'''}|j\rangle\langle i|e^{-i\boldsymbol{G}'\cdot\boldsymbol{r}'}|\mu)$$

$$\times\Bigg(\sum_i^{\text{occ}}\sum_j^{\text{emp}}\sum_k^{\text{occ}}\frac{1}{\epsilon_i - \epsilon_j + \epsilon_k - \omega} \tag{4.4}$$

$$+\sum_i^{\text{emp}}\sum_j^{\text{occ}}\sum_k^{\text{emp}}\frac{1}{\epsilon_i - \epsilon_j + \epsilon_k - \omega}\Bigg)\, v(\boldsymbol{G})v(\boldsymbol{G}') \tag{4.5}$$

The second-order self-energy has a energy dependence as well as the GW self-energy.

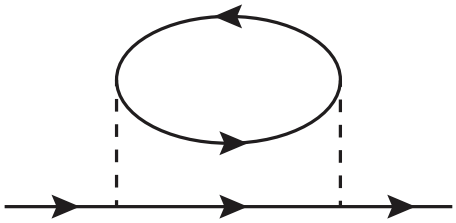

Fig.4.3: The Feynman diagrams of the second-order direct. The solid and dashed lines show Green's function and the bare Coulomb interaction, respectively.

However, it can be linearized the energy dependece as well as LGW, and the orthogonality and the completeness condition are satisfied.

4.2.1 Ward–Takahashi Identity

Ward–Takahashi identity is given by

$$\delta^4(x_1 - x)G^{-1}(x, x_2) - G^{-1}(x_1, x)\delta^4(x - x_2)$$

$$= i\nabla\cdot\boldsymbol{\Gamma}(x_1, x_2, x) + i\frac{\partial}{\partial t}\Gamma(x_1, x_2, x). \tag{4.6}$$

If we Fourier transform this equation with respect to $t - t_2$ and $t_1 - t$ into $\epsilon + \omega$ and ϵ, respectively, (i.e., if we multiply $\exp[i(\epsilon + \omega)(t - t_2) + i\epsilon(t_1 - t)]$ and integrate with respect to $t - t_1$ and $t_1 - t$), this equation becomes

$$\delta(\boldsymbol{r}_1 - \boldsymbol{r})G^{-1}(\boldsymbol{r}_1, \boldsymbol{r}_2; \epsilon + \omega) - G^{-1}(\boldsymbol{r}_1, \boldsymbol{r}_2; \epsilon)\delta(\boldsymbol{r} - \boldsymbol{r}_2)$$

$$= i\nabla\cdot\boldsymbol{\Gamma}(\boldsymbol{r}_1, \boldsymbol{r}_2, \boldsymbol{r}; \epsilon + \omega, \epsilon) + \omega\Gamma(\boldsymbol{r}_1, \boldsymbol{r}_2, \boldsymbol{r}; \epsilon + \omega, \epsilon). \tag{4.7}$$

At the lowest order, the first term in the right hand side is approximately given by

$$
\begin{aligned}
&i\nabla\cdot\mathbf{\Gamma}(\boldsymbol{r}_1,\boldsymbol{r}_2,\boldsymbol{r};\epsilon+\omega,\epsilon)\\
&\quad\sim\frac{1}{2}\nabla\cdot(\nabla_1+\nabla_2)\delta(\boldsymbol{r}_1-\boldsymbol{r})\delta(\boldsymbol{r}-\boldsymbol{r}_2)\\
&\quad=-\delta(\boldsymbol{r}_1-\boldsymbol{r})\frac{1}{2}\nabla^2\delta(\boldsymbol{r}-\boldsymbol{r}_2)+\frac{1}{2}\nabla_1^2\delta(\boldsymbol{r}_1-\boldsymbol{r})\delta(\boldsymbol{r}-\boldsymbol{r}_2)\\
&\qquad-i\int_{-\infty}^{\infty}\frac{d\omega'}{2\pi}G(\boldsymbol{r}_1,\boldsymbol{r};\epsilon-\omega')\left(-\frac{1}{2}\nabla^2\right)G(\boldsymbol{r},\boldsymbol{r}_2;\epsilon+\omega-\omega')V(\boldsymbol{r}_1-\boldsymbol{r}_2)\\
&\qquad+i\int_{-\infty}^{\infty}\frac{d\omega'}{2\pi}\left(-\frac{1}{2}\nabla_1^2\right)G(\boldsymbol{r}_1,\boldsymbol{r};\epsilon-\omega')G(\boldsymbol{r},\boldsymbol{r}_2;\epsilon+\omega-\omega')V(\boldsymbol{r}_1-\boldsymbol{r}_2).
\end{aligned}
\tag{4.8}
$$

Substituting this into (4.7), we have

$$
\begin{aligned}
&\delta(\boldsymbol{r}_1-\boldsymbol{r})G^{-1}(\boldsymbol{r}_1,\boldsymbol{r}_2;\epsilon+\omega)-G^{-1}(\boldsymbol{r}_1,\boldsymbol{r}_2;\epsilon)\delta(\boldsymbol{r}-\boldsymbol{r}_2)\\
&\quad=-\delta(\boldsymbol{r}_1-\boldsymbol{r})\frac{1}{2}\nabla^2\delta(\boldsymbol{r}-\boldsymbol{r}_2)+\frac{1}{2}\nabla_1^2\delta(\boldsymbol{r}_1-\boldsymbol{r})\delta(\boldsymbol{r}-\boldsymbol{r}_2)\\
&\qquad-i\int_{-\infty}^{\infty}\frac{d\omega'}{2\pi}G(\boldsymbol{r}_1,\boldsymbol{r};\epsilon-\omega')\left(-\frac{1}{2}\nabla^2\right)G(\boldsymbol{r},\boldsymbol{r}_2;\epsilon+\omega-\omega')V(\boldsymbol{r}_1-\boldsymbol{r}_2)\\
&\qquad+i\int_{-\infty}^{\infty}\frac{d\omega'}{2\pi}\left(-\frac{1}{2}\nabla_1^2\right)G(\boldsymbol{r}_1,\boldsymbol{r};\epsilon-\omega')G(\boldsymbol{r},\boldsymbol{r}_2;\epsilon+\omega-\omega')V(\boldsymbol{r}_1-\boldsymbol{r}_2)\\
&\qquad+\omega\Gamma(\boldsymbol{r}_1,\boldsymbol{r}_2,\boldsymbol{r};\epsilon+\omega,\epsilon),
\end{aligned}
\tag{4.9}
$$

which is equivalent to

$$
\begin{aligned}
&\Sigma(\boldsymbol{r}_1,\boldsymbol{r}_2;\epsilon)\delta(\boldsymbol{r}-\boldsymbol{r}_2)-\delta(\boldsymbol{r}_1-\boldsymbol{r})\Sigma(\boldsymbol{r}_1,\boldsymbol{r}_2;\epsilon+\omega)\\
&\quad=-i\int_{-\infty}^{\infty}\frac{d\omega'}{2\pi}G(\boldsymbol{r}_1,\boldsymbol{r};\epsilon-\omega')\left(-\frac{1}{2}\nabla^2\right)G(\boldsymbol{r},\boldsymbol{r}_2;\epsilon+\omega-\omega')V(\boldsymbol{r}_1-\boldsymbol{r}_2)\\
&\qquad+i\int_{-\infty}^{\infty}\frac{d\omega'}{2\pi}\left(-\frac{1}{2}\nabla_1^2\right)G(\boldsymbol{r}_1,\boldsymbol{r};\epsilon-\omega')G(\boldsymbol{r},\boldsymbol{r}_2;\epsilon+\omega-\omega')V(\boldsymbol{r}_1-\boldsymbol{r}_2)\\
&\qquad+\omega[\Gamma(\boldsymbol{r}_1,\boldsymbol{r}_2,\boldsymbol{r};\epsilon+\omega,\epsilon)-\delta(\boldsymbol{r}_1-\boldsymbol{r})\delta(\boldsymbol{r}-\boldsymbol{r}_2)],
\end{aligned}
\tag{4.10}
$$

Then, using the self-energy in the linearized GW formulation, we can rewrite the left hand side of (4.10) as

$$
\begin{aligned}
&i\int_{-\infty}^{\infty}\frac{d\omega'}{2\pi}[\widetilde{G}(\boldsymbol{r}_1,\boldsymbol{r}_2;\epsilon-\omega')\delta(\boldsymbol{r}-\boldsymbol{r}_2)-\delta(\boldsymbol{r}_1-\boldsymbol{r})\widetilde{G}(\boldsymbol{r}_1,\boldsymbol{r}_2;\epsilon+\omega-\omega')]\widetilde{W}(\boldsymbol{r}_1,\boldsymbol{r}_2;\omega')\\
&\quad=i\int_{-\infty}^{\infty}\frac{d\omega'}{2\pi}\Bigg[\langle\boldsymbol{r}_1|\frac{1}{\epsilon-\omega'-\widetilde{H}-i\delta_{\widetilde{H}}}|\boldsymbol{r}\rangle\langle\boldsymbol{r}|\boldsymbol{r}_2\rangle\\
&\qquad-\langle\boldsymbol{r}_1|\boldsymbol{r}\rangle\langle\boldsymbol{r}|\frac{1}{\epsilon+\omega-\omega'-\widetilde{H}-i\delta_{\widetilde{H}}}|\boldsymbol{r}_2\rangle\Bigg]\widetilde{W}(\boldsymbol{r}_1,\boldsymbol{r}_2;\omega')\\
&\quad=i\int_{-\infty}^{\infty}\frac{d\omega'}{2\pi}\Bigg[\langle\boldsymbol{r}_1|\frac{1}{\epsilon-\omega'-\widetilde{H}-i\delta_{\widetilde{H}}}|\boldsymbol{r}\rangle\langle\boldsymbol{r}|\frac{\omega}{\epsilon+\omega-\omega'-\widetilde{H}-i\delta_{\widetilde{H}}}|\boldsymbol{r}_2\rangle
\end{aligned}
$$

$$
\begin{aligned}
&- \langle \boldsymbol{r}_1 | \frac{1}{\epsilon - \omega' - \widetilde{H} - i\delta_{\widetilde{H}}} | \boldsymbol{r} \rangle \langle \boldsymbol{r} | \widetilde{H} \frac{1}{\epsilon + \omega - \omega' - \widetilde{H} - i\delta_{\widetilde{H}}} | \boldsymbol{r}_2 \rangle \\
&+ \langle \boldsymbol{r}_1 | \widetilde{H} \frac{1}{\epsilon - \omega' - \widetilde{H} - i\delta_{\widetilde{H}}} | \boldsymbol{r} \rangle \langle \boldsymbol{r} | \frac{1}{\epsilon + \omega - \omega' - \widetilde{H} - i\delta_{\widetilde{H}}} | \boldsymbol{r}_2 \rangle \Big] \widetilde{W}(\boldsymbol{r}_1, \boldsymbol{r}_2; \omega') \\
= i \int_{-\infty}^{\infty} \frac{d\omega'}{2\pi} \Big[& \omega \widetilde{G}(\boldsymbol{r}_1, \boldsymbol{r}; \epsilon - \omega') \widetilde{G}(\boldsymbol{r}, \boldsymbol{r}_2; \epsilon + \omega - \omega') \\
&- \widetilde{G}(\boldsymbol{r}_1, \boldsymbol{r}; \epsilon - \omega') \left(-\frac{1}{2} \nabla^2 \right) \widetilde{G}(\boldsymbol{r}, \boldsymbol{r}_2; \epsilon + \omega - \omega') \\
&+ \left(-\frac{1}{2} \nabla_1^2 \right) \widetilde{G}(\boldsymbol{r}_1, \boldsymbol{r}; \epsilon - \omega') \widetilde{G}(\boldsymbol{r}, \boldsymbol{r}_2; \epsilon + \omega - \omega') \\
&- \widetilde{G}(\boldsymbol{r}_1, \boldsymbol{r}; \epsilon - \omega') \Sigma_{\mathrm{xc}}(\boldsymbol{r}, \boldsymbol{r}') \widetilde{G}(\boldsymbol{r}', \boldsymbol{r}_2; \epsilon + \omega - \omega') \\
&+ \Sigma_{\mathrm{xc}}(\boldsymbol{r}_1, \boldsymbol{r}') \widetilde{G}(\boldsymbol{r}', \boldsymbol{r}; \epsilon - \omega') \widetilde{G}(\boldsymbol{r}, \boldsymbol{r}_2; \epsilon + \omega - \omega') \Big] \widetilde{W}(\boldsymbol{r}_1, \boldsymbol{r}_2; \omega'), \quad (4.11)
\end{aligned}
$$

where we used the fact that the electron-nucleus potential in $\widetilde{H}$ commutes with the operator $|\boldsymbol{r}\rangle\langle\boldsymbol{r}|$. Equation (4.11) is exactly equal to the lowest order vertex part shown in Fig.4.1 in the lowest order in the electron-electron Coulomb interaction V, since $\widetilde{G}$ and $\widetilde{W}(\boldsymbol{r}_1, \boldsymbol{r}_2; \omega')$ can be replaced by G and $V(\boldsymbol{r}_1 - \boldsymbol{r}_2)$, respectively, in the lowest order approximation, the second and the third terms cancel with the first and second terms of the right hand side of Eq. (4.10), and the fourth and fifth terms are clearly the second order in V and thus can be ignored. Therefore, our formulation satisfies the Ward–Takahashi identity in the lowest order approximation.

In the GWΓ approach, the first-order vertex correction is included in not only the self-energy but also the polarization function. The polarization function with the first-order vertex correction can be written as

$$
\begin{aligned}
P^{GW\Gamma}(\boldsymbol{r}, \boldsymbol{r}', \omega) = -i^2 \iint & G(\boldsymbol{r}, \boldsymbol{r}_1, \omega + \omega') G(\boldsymbol{r}, \boldsymbol{r}_2, \omega') \\
& \times \Gamma(\boldsymbol{r}_1, \boldsymbol{r}_2, \boldsymbol{r}, \omega'', \omega) d\omega' d\omega'' d\boldsymbol{r}_1 d\boldsymbol{r}_2. \quad (4.12)
\end{aligned}
$$

The dynamically screened interaction W is constructed by the polarization function P as with the GW approximation:

$$
\begin{aligned}
W^{GW\Gamma}(\boldsymbol{r}, \boldsymbol{r}', \omega) &= \int \epsilon^{-1}(\boldsymbol{r}, \boldsymbol{r}_1, \omega) v(\boldsymbol{r}_1 - \boldsymbol{r}') d\boldsymbol{r}_1 \\
&= \int \left(\delta(\boldsymbol{r} - \boldsymbol{r}_2) - \int v(\boldsymbol{r} - \boldsymbol{r}_1) \left(P^{GW}(\boldsymbol{r}_1, \boldsymbol{r}_2, \omega) + P^{GW\Gamma}(\boldsymbol{r}_1, \boldsymbol{r}_2, \omega) \right) d\boldsymbol{r}_1 \right) \\
&\quad \times v(\boldsymbol{r}_2 - \boldsymbol{r}') d\boldsymbol{r}_1 d\boldsymbol{r}_2. \quad (4.13)
\end{aligned}
$$

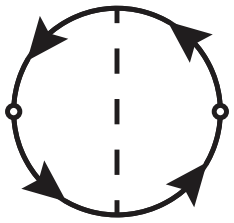

Fig.4.4: The Feynman diagrams of the polarization function with the first order vertex correction. The solid and dashed lines show Green's function and the bare Coulomb interaction, respectively.

The Fourier transformation of $P^{GW\Gamma}(\boldsymbol{r}_1, \boldsymbol{r}_2, \omega)$ can be evaluate as follows:

$$\begin{aligned}
P^{GW\Gamma}_{\boldsymbol{G},\boldsymbol{G}'}(\omega) = -\frac{i^2}{\Omega}\sum_{i,j,k,l}\sum_{\boldsymbol{G}''}\iint\frac{d\omega'}{2\pi}\frac{d\omega''}{2\pi} \\
\times\frac{\langle l|e^{i\boldsymbol{G}\cdot\boldsymbol{r}}|i\rangle\langle i|e^{i\boldsymbol{G}''\cdot\boldsymbol{r}''}|j\rangle\langle j|e^{-i\boldsymbol{G}'\cdot\boldsymbol{r}'}|k\rangle\langle k|e^{-i\boldsymbol{G}''\cdot\boldsymbol{r}'''}|l\rangle}{(\omega+\omega''-(\epsilon_i+i\eta_i))(\omega+\omega''-\omega'-(\epsilon_j+i\eta_j))} \\
\times\frac{v(\boldsymbol{G}'')}{(\omega''-\omega'-(\epsilon_k+i\eta_k))(\omega''-(\epsilon_l+i\eta_l))} \\
=\frac{1}{\Omega}\sum_{\boldsymbol{G}''}\langle l|e^{i\boldsymbol{G}\cdot\boldsymbol{r}}|i\rangle\langle i|e^{i\boldsymbol{G}''\cdot\boldsymbol{r}''}|j\rangle\langle j|e^{-i\boldsymbol{G}'\cdot\boldsymbol{r}'}|k\rangle\langle k|e^{-i\boldsymbol{G}''\cdot\boldsymbol{r}'''}|l\rangle \\
\times\left(\sum_i^{\mathrm{occ}}\sum_l^{\mathrm{emp}}\frac{1}{\epsilon_i-\epsilon_l-\omega+i\eta}-\sum_i^{\mathrm{emp}}\sum_l^{\mathrm{occ}}\frac{1}{\epsilon_i-\epsilon_l-\omega-i\eta}\right) \\
\times\left(\sum_j^{\mathrm{emp}}\sum_k^{\mathrm{occ}}\frac{1}{\epsilon_j-\epsilon_k-\omega-i\eta}-\sum_j^{\mathrm{occ}}\sum_k^{\mathrm{emp}}\frac{1}{\epsilon_j-\epsilon_k-\omega+i\eta}\right)v(\boldsymbol{G}'') \qquad (4.14)
\end{aligned}$$

The GWΓ self-energy can be written as

$$\begin{aligned}
(\nu|\Sigma_{GW\Gamma}(\omega)|\mu) = (\nu|\Sigma_{GW}(\omega)|\mu) \\
+\frac{i^2}{\Omega}\sum_{i,j,k}\sum_{\boldsymbol{G},\boldsymbol{G}',\boldsymbol{G}''}\iint\frac{d\omega'}{2\pi}\frac{d\omega''}{2\pi} \\
\times\frac{(\nu|e^{i\boldsymbol{G}\cdot\boldsymbol{r}}|i\rangle\langle i|e^{i\boldsymbol{G}''\cdot\boldsymbol{r}''}|j\rangle\langle j|e^{-i\boldsymbol{G}'\cdot\boldsymbol{r}'''}|k\rangle\langle k|e^{-i\boldsymbol{G}''\cdot\boldsymbol{r}'}|\mu)}{\omega-\omega'-(\epsilon_i+i\eta_i)} \\
\times\frac{W^{GW\Gamma}_{\boldsymbol{G},\boldsymbol{G}'}(\omega')v(\boldsymbol{G}'')}{(\omega-\omega'-\omega''-(\epsilon_j+i\eta_j))(\omega-\omega''-(\epsilon_k+i\eta_k))}. \qquad (4.15)
\end{aligned}$$

This self-energy can be divided into three terms as

$$(\nu|\Sigma_{GW\Gamma}(\omega)|\mu) = (\nu|\Sigma_{GW}(\omega)|\mu) + (\nu|\Sigma_{GV\Gamma}(\omega)|\mu) + (\nu|\Sigma_{GX\Gamma}(\omega)|\mu). \qquad (4.16)$$

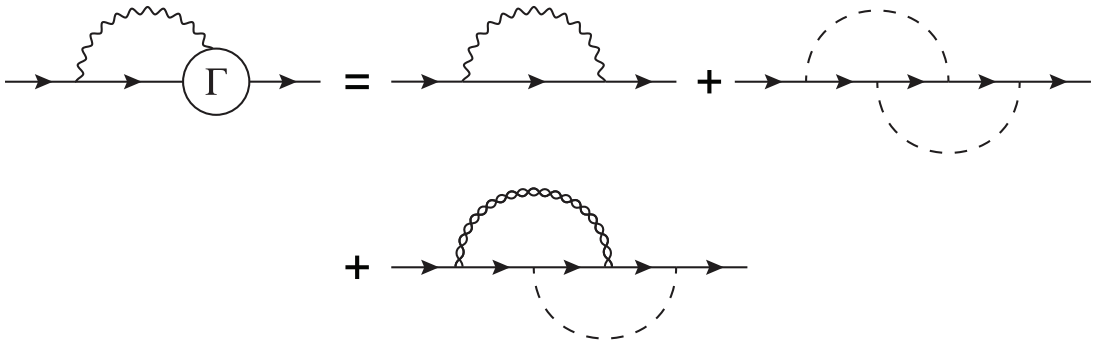

Fig.4.5: The Feynman diagrams of the GWΓ self-energy. The solid, dashed, and wiggly lines show Green's function, the bare Coulomb interaction, the dynamically screened interaction, respectively. The bubbly line is defined as Fig.4.6.

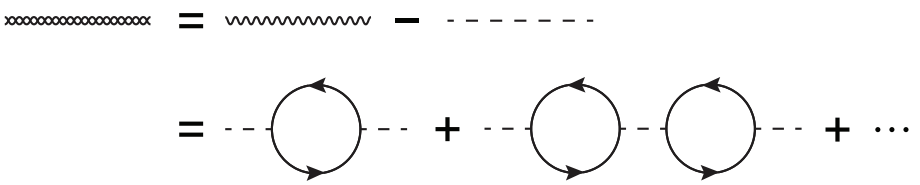

Fig.4.6: The bubbly line is defined as the interaction which the dynamically screened interaction minus the bare Coulomb interaction.

Eq.(4.16) can be diagrammatically represented as Fig.4.5. Here the first term is just the GW self-energy, the second term is the second-order exchange, and the third term is the higher-order correction term. In order to evaluate the third term as well as the first term, we use the von der Linden-Horsch (vdLH) plasmon-pole model. It makes the calculation of Eq.(4.15) possible within a reasonable computational time. The third term with vdLH plasmon-pole model can be written as

$$
\begin{aligned}
(\nu|\Sigma_{GX\Gamma}(\omega)|\mu) = \frac{i}{\Omega}\sum_i \sum_{\boldsymbol{G},\boldsymbol{G}',\boldsymbol{G}''}\sum_p \int \frac{d\omega'}{2\pi}\frac{4\pi z_p \omega_p^2 v(\boldsymbol{G}'')}{(\omega-\omega'-(\epsilon_i+i\eta_i))(\omega'^2-(\omega_p-i\eta)^2)} \\
\times \Theta_p(\boldsymbol{G})(\nu|e^{i\boldsymbol{G}\cdot\boldsymbol{r}}|i\rangle\langle j|e^{-i\boldsymbol{G}'\cdot\boldsymbol{r}'''}|k\rangle \\
\times \Theta_p^*(\boldsymbol{G}')\langle i|e^{i\boldsymbol{G}''\cdot\boldsymbol{r}''}|j\rangle\langle k|e^{-i\boldsymbol{G}''\cdot\boldsymbol{r}'}|\mu) \\
\times \left(\sum_j^{\text{occ}}\sum_k^{\text{emp}}\frac{1}{\epsilon_k-\epsilon_j-\omega'-i\eta} - \sum_j^{\text{emp}}\sum_k^{\text{occ}}\frac{1}{\epsilon_k-\epsilon_j-\omega'+i\eta}\right) \\
= \frac{i}{\Omega}\sum_i\sum_p 2\pi z_p \int \frac{d\omega'}{2\pi}\frac{\beta_{p,\nu,i}\beta^*_{p,j,k}U_{i,j,k,\mu}}{\omega-\omega'-(\epsilon_i+i\eta_i)}
\end{aligned}
$$

$$
\begin{aligned}
&\times \left(\frac{1}{\omega' - (\omega_p - i\eta)} - \frac{1}{\omega' + (\omega_p - i\eta)} \right) \\
&\times \left(\sum_j^{\text{occ}} \sum_k^{\text{emp}} \frac{1}{\epsilon_k - \epsilon_j - \omega' - i\eta} - \sum_j^{\text{emp}} \sum_k^{\text{occ}} \frac{1}{\epsilon_k - \epsilon_j - \omega' + i\eta} \right) \\
= \frac{2\pi}{\Omega} &\sum_p z_p \beta_{p,\nu,i} \beta^*_{p,j,k} U_{i,j,k,\mu} \\
&\times \Bigg[\sum_i^{\text{occ}} \sum_j^{\text{occ}} \sum_k^{\text{emp}} \frac{1}{\omega - (\epsilon_i + i\eta) + \omega_p} \frac{1}{(\epsilon_i + i\eta) - \epsilon_j + \epsilon_k - \omega} \\
&+ \sum_i^{\text{emp}} \sum_j^{\text{occ}} \sum_k^{\text{emp}} \frac{1}{\omega - (\epsilon_i + i\eta) - \omega_p} \frac{1}{(\epsilon_i + i\eta) - \epsilon_j + \epsilon_k - \omega} \\
&- \sum_i^{\text{all}} \sum_j^{\text{occ}} \sum_k^{\text{emp}} \frac{1}{\epsilon_k - \epsilon_j - i\eta + \omega_p} \frac{1}{(\epsilon_i + i\eta_i) - \epsilon_j + \epsilon_k - \omega} \\
&- \sum_i^{\text{occ}} \sum_j^{\text{emp}} \sum_k^{\text{occ}} \frac{1}{\omega - (\epsilon_i + i\eta) + \omega_p} \frac{1}{(\epsilon_i + i\eta) - \epsilon_j + \epsilon_k - \omega} \\
&- \sum_i^{\text{emp}} \sum_j^{\text{emp}} \sum_k^{\text{occ}} \frac{1}{\omega - (\epsilon_i + i\eta) - \omega_p} \frac{1}{(\epsilon_i + i\eta) - \epsilon_j + \epsilon_k - \omega} \\
&+ \sum_i^{\text{all}} \sum_j^{\text{emp}} \sum_k^{\text{occ}} \frac{1}{\epsilon_k - \epsilon_j + i\eta - \omega_p} \frac{1}{(\epsilon_i + i\eta_i) - \epsilon_j + \epsilon_k - \omega} \Bigg],
\end{aligned}
\tag{4.17}
$$

where

$$
U_{i,j,k,\mu} = \sum_{\boldsymbol{G}''} \langle i | e^{i\boldsymbol{G}''\cdot\boldsymbol{r}''} | j \rangle \langle k | e^{-i\boldsymbol{G}''\cdot\boldsymbol{r}'} | \mu \rangle, \tag{4.18}
$$

$$
\beta_{p,\nu,i} = \sum_{\boldsymbol{G}} \Theta_p(\boldsymbol{G}) (\nu | e^{i\boldsymbol{G}\cdot\boldsymbol{r}} | i \rangle, \tag{4.19}
$$

$$
\gamma_{p,k,j} = \sum_{\boldsymbol{G}} \Theta_p(\boldsymbol{G} \langle k | e^{i\boldsymbol{G}\cdot\boldsymbol{r}} | j \rangle. \tag{4.20}
$$

4.2.2 Bethe-Sapleter Equation

In order to obtain accurate optical spectra, it is neccesarily to include excitonic effects by introducing two-particle Green's function for electrons and holes. The Bethe-

Sapleter equation is given by

$$L^{\sigma_1\sigma_2}_{\sigma_1'\sigma_2'}(x_1, x_1'; x_2, x_2') = G_{\sigma_1\sigma_2}(x_1, x_2)G_{\sigma_2'\sigma_1'}(x_2', x_1') + \sum_{\sigma_3\sigma_3'}\sum_{\sigma_4\sigma_4'}\int G_{\sigma_1\sigma_3}(x_1, x_3)\Xi^{\sigma_3\sigma_4}_{\sigma_3'\sigma_4'}(x_3, x_3'; x_4, x_4')G_{\sigma_3'\sigma_1'}(x_3', x_1') \times L^{\sigma_4\sigma_2}_{\sigma_4'\sigma_2'}(x_4, x_4'; x_2, x_2')d^4x_3 d^4x_3' d^4x_4 d^4x_4', \tag{4.21}$$

where σ_n is the spin state for the particle at x_n, L is two-particle Green's function apart from the two one-particle Green's fucntions, and the integration kernel Ξ is defined as

$$\Xi^{\sigma_3\sigma_4}_{\sigma_3'\sigma_4'}(x_3, x_3'; x_4, x_4') = \frac{\delta\Sigma_{\sigma_3\sigma_3'}(x_3, x_3')}{\delta G_{\sigma_4\sigma_4'}(x_4, x_4')}. \tag{4.22}$$

In the GW approximation, Eq.(4.22) can be given by

$$\Xi^{\sigma_3\sigma_4}_{\sigma_3'\sigma_4'}(x_3, x_3'; x_4, x_4') = -i\delta_{\sigma_3\sigma_3'}\delta_{\sigma_4\sigma_4'}\delta^4(x_3 - x_3')\delta^4(x_4 - x_4')v(\boldsymbol{r}_3 - \boldsymbol{r}_4) + i\delta_{\sigma_3\sigma_4}\delta_{\sigma_3'\sigma_4'}\delta^4(x_3 - x_4)\delta^4(x_3' - x_4')W'(x_3, x_3'). \tag{4.23}$$

Here, W' includes the higher-order terms derived from the functional derivative of G in the ring diagrams of W. Howerver, in general these terms is neglected and W' is replaced by the dynamically screened interaction W within the RPA. Equation (4.22) is diagrammatically given by Solving Eq.(4.21) is equivalent to solve the following

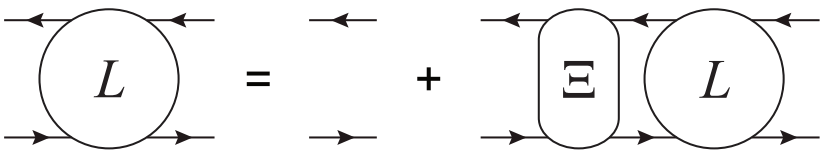

Fig.4.7: The Feynman diagram of the Bethe-Salpeter equation.

eigenvalue problem:

$$\sum_{\mu',\nu'} H_{\mu\nu;\mu'\nu'}A_{\mu'\nu'} = \Omega A_{\mu\nu}. \tag{4.24}$$

For simplicity, the indices for spin states are omitted. Here, the matrix $H_{\mu\nu;\mu',\nu'}$ is given by

$$H_{\mu\nu;\mu'\nu'} = \delta_{\mu,\mu'}\delta_{\nu,\nu'}(\epsilon_\nu - \epsilon_\mu) + 2V_{\mu\nu;\mu'\nu'}\delta_{M,0} - W_{\mu\nu;\mu'\nu'}(\Omega), \tag{4.25}$$

where ϵ_μ and ϵ_ν are the quasiparticle energies of electrons and holes, $V_{\mu\nu;\mu'\nu'}$ and $W_{\mu\nu;\mu'\nu'}$ are the exchange and direct term defined as

$$V^{\sigma_1;\sigma_2}_{\mu\nu;\mu'\nu'} = \int \phi^*_{\mu\sigma_1}(\boldsymbol{r}_3)\phi_{\nu\sigma_1}(\boldsymbol{r}_3)v(\boldsymbol{r}_3-\boldsymbol{r}_4)\phi_{\mu'\sigma_2}(\boldsymbol{r}_4)\phi^*_{\nu'\sigma_2}(\boldsymbol{r}_4)d\boldsymbol{r}_3 d\boldsymbol{r}_4 \tag{4.26}$$

$$\begin{aligned} W^{\sigma_1;\sigma_1'}_{\mu\nu;\mu'\nu'}(\Omega) = i\int \frac{d\omega}{2\pi}\phi^*_{\mu\sigma_1}(\boldsymbol{r}_3)\phi_{\nu\sigma_1'}(\boldsymbol{r}_3')W(\boldsymbol{r}_3,\boldsymbol{r}_3';\omega)\phi_{\mu'\sigma_1}(\boldsymbol{r}_3)\phi^*_{\nu'\sigma_1'}(\boldsymbol{r}_3')d\boldsymbol{r}_3 d\boldsymbol{r}_3' \\ \times\left[\frac{i}{\Omega-\omega-(\epsilon_{\mu'\sigma_1}-\epsilon_{\nu\sigma_1'})+i0^+}+\frac{i}{\Omega+\omega-(\epsilon_{\mu\sigma_1}-\epsilon_{\nu'\sigma_1'})+i0^+}\right]. \end{aligned} \tag{4.27}$$

The exchange term appears only for a singlet state ($M = 0$), and the direct term can be evaluated with the plasmon-pole models. Finally, the eigenvalues Ω and eigenfunctions $A_{\mu\nu}$ of Eq.(4.24) give the excitation energies and the oscillator strength, respectively.

4.2.3 Total Energy

The Feynman diagram of the Luttinger–Ward functional for the second-order exchange is shown in Fig.4.8, and it can be evaluated as

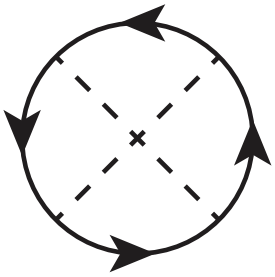

Fig.4.8: The Feynman diagram of the second-order exchange.

$$\begin{aligned} \Phi_{\text{2nd exchange}}[\widetilde{G}] &= -\frac{1}{2}\int_0^1 \frac{d\lambda}{\lambda}\mathrm{Tr}\left[\Sigma_{\mathrm{GV\Gamma}}[\widetilde{G}]\widetilde{G}\right] \\ &= -\frac{i}{2}\int_0^1 \frac{d\lambda}{\lambda}\int\frac{d\omega}{2\pi}\sum_n \langle\widetilde{n}|\Sigma_{\mathrm{GV\Gamma}}(\omega)\widetilde{G}(\omega)|\widetilde{n}\rangle \\ &= -\frac{i}{2\Omega}\int_0^1 \frac{d\lambda}{\lambda}\int\frac{d\omega}{2\pi}\sum_n\sum_{\boldsymbol{G},\boldsymbol{G}'} \\ &\quad\times\frac{\langle\widetilde{n}|e^{i\boldsymbol{G}\cdot\boldsymbol{r}}|i\rangle\langle i|e^{i\boldsymbol{G}'\cdot\boldsymbol{r}''}|j\rangle\langle j|e^{-i\boldsymbol{G}\cdot\boldsymbol{r}'''}|k\rangle\langle k|e^{-i\boldsymbol{G}'\cdot\boldsymbol{r}'}|\widetilde{n}\rangle}{\omega-\epsilon_n-i\eta_n} \end{aligned}$$

$$\times \Bigg(\sum_{i}^{\text{occ}} \sum_{j}^{\text{emp}} \sum_{k}^{\text{occ}} \frac{1}{\epsilon_i - \epsilon_j + \epsilon_k - \omega + i\eta} + \sum_{i}^{\text{emp}} \sum_{j}^{\text{occ}} \sum_{k}^{\text{emp}} \frac{1}{\epsilon_i - \epsilon_j + \epsilon_k - \omega - i\eta} \Bigg) \lambda^2 v(\boldsymbol{G}) v(\boldsymbol{G}')$$

$$= \frac{1}{4\Omega} \sum_{\boldsymbol{G},\boldsymbol{G}'} \langle \widetilde{n} | e^{i\boldsymbol{G}\cdot\boldsymbol{r}} | i \rangle \langle i | e^{i\boldsymbol{G}'\cdot\boldsymbol{r}''} | j \rangle \langle j | e^{-i\boldsymbol{G}\cdot\boldsymbol{r}'''} | k \rangle \langle k | e^{-i\boldsymbol{G}'\cdot\boldsymbol{r}'} | \widetilde{n} \rangle$$

$$\times \Bigg(\sum_{n}^{\text{occ}} \sum_{i}^{\text{emp}} \sum_{j}^{\text{occ}} \sum_{k}^{\text{emp}} \frac{1}{\epsilon_n - \epsilon_i + \epsilon_j - \epsilon_k - i\eta} - \sum_{n}^{\text{emp}} \sum_{i}^{\text{occ}} \sum_{j}^{\text{emp}} \sum_{k}^{\text{occ}} \frac{1}{\epsilon_n - \epsilon_i + \epsilon_j - \epsilon_k + i\eta} \Bigg) v(\boldsymbol{G}) v(\boldsymbol{G}'). \quad (4.28)$$

Therefore, the total energy of GWΓ is given by

$$E_{\text{G}}^N = T + V_{\text{n-e}} + \Phi[\widetilde{G}] + E_{\text{Ewald}} \quad (4.29)$$

$$= T + V_{\text{n-e}} + \Phi_c[\widetilde{G}] + \Phi_{\text{c}}[\widetilde{G}] + \Phi_{\text{2nd exchange}}[\widetilde{G}] + E_{\text{Ewald}} \quad (4.30)$$

$$(4.31)$$

where T is the kinetic energy, $V_{\text{n-e}}$ is the nucleus-electron Coulomb energy, the E_{Ewald} is Coulombic energy between nuclei, and $\Phi_c[\widetilde{G}]$ is the GW correlation part of the Luttinger–Ward functional given by Eq.(3.30).

4.3 Methodology

We chose simple isolated Li and Na systems to validate the GWΓ approach. For clusters composed of odd number of atoms, we performed spin-dependent calculations. The structures of clusters were optimized with the B3LYP functional available in DMol^3 package.

We used the all-electron mixed basis approach, where the one particle wave functions are expanded with the combination of plane waves and atomic orbitals. This approach can describe both deep core states and plane-wave-like continuous states efficiently and appropriately compared to the approaches which use only plane waves or only localized orbitals as basis functions.

The spherical cut technique is used to ignore the interaction with the periodic images. The atoms and dimers are put in the rhombohedral unit cell with $a = b = c = 16$ Å and $\alpha = \beta = \gamma = 60°$. The cutoff energy for the plane waves and $\boldsymbol{G}$, $\boldsymbol{G}'$ in the

correlation term is 4.32 Ry, and the cutoff energy for $\boldsymbol{G}$ in the Fock exchange term is 38.87 Ry.

4.4 Results and Discussion

The absolute values of the total energy E_{G}^{N} calculated with GW, LGW, and GWΓ in atomic units (a.u.) (1 a.u. = 27.2 eV) of Li and Li_2 (at the equilibrium distance for dimers) are shown in Table 4.1 together with virial ratio $-V/T$ and components contributing to the total energy.

Table.4.1: Total energies (E_{G}^{N}), their components in units of a.u. (1 a.u. = 27.2 eV), and virial ratios ($-V/T$) calculated by various approaches. The components, T, $V_{\text{n-e}}$, V_{H}, V_{x}, and Φ_{c} are the kinetic energy, the nucleus-electron Coulomb energy, Hartree energy, the Fock exchange energy, and the correlation energy, respectively.

		E_{G}^{N}	T	$V_{\text{n-e}}$	V_{H}	V_{x}	Φ_{c}	$-V/T$
Li	GW	−7.4423	7.4408	−17.1581	4.0659	−1.7812	−0.0097	2.000
	LGW	−7.4427	7.4763	−17.1989	4.0764	−1.7864	−0.0101	1.995
	GWΓ	−7.4336	7.4858	−17.2018	4.0700	−1.7864	−0.0012	1.993
Li_2	GW	−14.9051	14.8879	−36.4393	9.2405	−3.5574	−0.0334	2.001
	LGW	−14.9073	14.9818	−36.5483	9.2705	−3.5715	−0.0360	1.997
	GWΓ	−14.8867	14.9943	−36.5478	9.2591	−3.5720	−0.0157	1.993

As the contribution of the correlation energy from the second-order exchange term is positive, The total energy caculated by GWΓ is greater than that of GW and LGW. However, this result seems reasonable because the second exchange term of the correlation energy for the electron gas is also positive.

The results for the ionization potential (IP), which is equal to $-\epsilon_{\mathrm{HOMO}}$, and the electron affinity (EA), which is equal to $-\epsilon_{\mathrm{LUMO}}$, of Li, Li_2 calculated with the self-consistent GW (GW), the linearized self-consistent GW (LGW), and GWΓ are summarized in Table.4.2 together with experimental data [52–54] in units of eV.

The ionization potentials calculated by GWΓ for Li and Li_2 are slightly underestimated compared to the experimental data, and the electron affinities of that are improved and show good agreement with the experimental data. As a result, GWΓ improves the tendency that GW and LGW overestimate the energy gap. The underestimation of the ionization potential within GWΓ is probably due to the neglect of the higher-order vertex correction.

Table.4.2: Ionization potentials (IP) and electron affinities (EA) in eV of Li and Li_2.

	Li		Li_2	
	IP	EA	IP	EA
GW	5.78	0.22	5.56	0.20
LGW	5.65	0.28	5.32	0.35
GWΓ	5.13	0.57	4.91	0.46
Expt.	5.39[a]	0.62[b]	5.15[a]	0.44[c]

[a] See Ref. [52].
[b] See Ref. [53].
[c] See Ref. [54].

The optical absorption spectra for Na_2 obtained by LGW and GWΓ are shown in Fig.4.9.

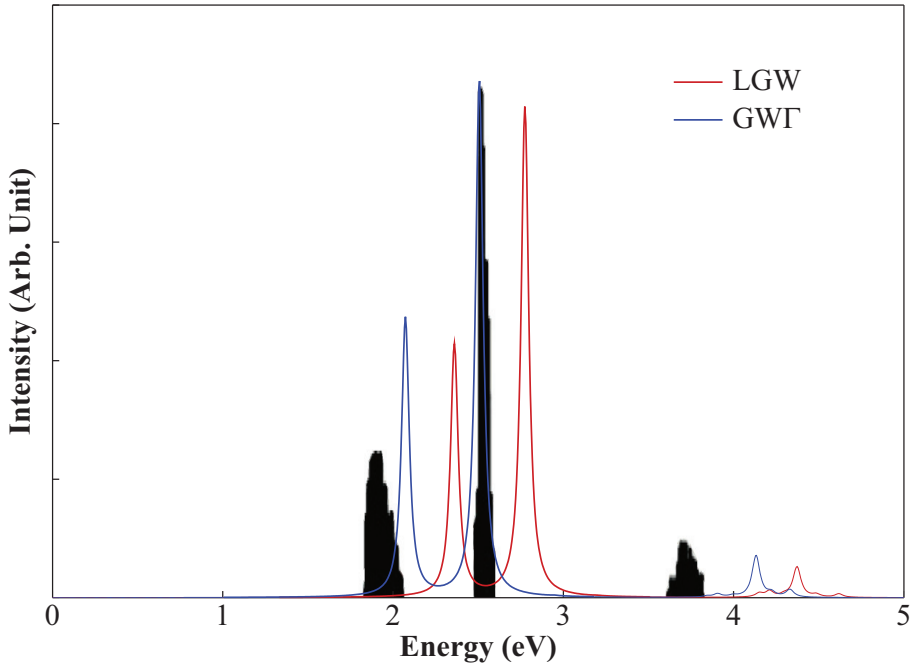

Fig.4.9: The optical absorpption spectra for Na_2 obtained by LGW (red line) and GWΓ (blue line) together with the experimental spectrum (black line).

The shapes of the spectra are similar between LGW and GWΓ, but the peak positions are fairly different. The spectrum obtained by GWΓ shows excellent agreement

with the experimental spectrum. As a result of GWΓ improves the energy gap, the optical spectrum calculated by GWΓ is also improved.

Chapter 5

Summary

I have implemented the self-consistent GW, the linearized GW, and GWΓ approaches in the all-electron mixed basis program TOMBO.

In the second chapter, I have shown the total energy as well as its kinetic- and potential-energy contributions of isolated He, Be, Ne, Mg, Ar, and Ca atoms obtained by the self-consistent LDA, HF, and GW calculations using the all-electron mixed basis approach. The resulting virial ratio is in fairly good agreement with the exact value 2 in all the cases. I have compared the resulting HOMO and LUMO energies among the LDA, HF, and GW calculations and with the available experimental data. I have found that the HOMO energy, i.e., the negative of the IP, is in excellent agreement with the experimental data only in the GW calculation. I have depicted the LUMO wave functions of noble gas atoms and found that they are resonating virtual bound states. The LUMO wave function of GW spreads wider than that of LDA and thinner than that of HF. I also have calculated the total energy and their components as well as the quasiparticle energies of spin polarized or unpolarized diatomic molecules (dimers), B_2, Al_2, and Si_2. According to our GWA result, the triplet state is more stable than the singlet state in B_2, Al_2, and Si_2. The difference in the exchange-correlation energy, $V_x + \Phi_c$, between the triplet and singlet states roughly corresponds to the total energy difference, although a correspondence is not observed in all the other contributions (T, $V_{n\text{-}e}$, and V_H). The resulting quasiparticle energies, corresponding to the ionization potential and the electron affinity, are comparable with the available experimental data.

In the third chapter, I proposed a linearized self-consistent GW approach. The important advantages of this approach are (1) the Ward identity (Ward–Takahashi identity in the limit of $\boldsymbol{q} = 0$ and $\omega - \omega' = 0$) is satisfied, (2) the vertex correction

is included within this identity, and (3) the non-Hermitian problem is resolved by the renormalization of Green's function. As a result, I confirmed that this approach greatly improves the IP and EA of not only LDA, HF, and B3LYP approaches but also the non-linearized self-consistent GW approach. I also proposed convenient formulae to evaluate the Luttinger–Ward functional and calculated the ground-state total energy of Li, Li_2, Na, and Na_2. For Li_2, I estimated the equilibrium bond length, the binding energy, the bond force constant, and the vibrational frequency within GW and LGW. Although the resulting binding energy and vibration frequency are somewhat smaller than the preexisting experimental values, I expect that they will reproduce correctly the long distance behavior in a van der Waals regime.

In the fourth chapter, I give the detailed formulation of the GWΓ approach, where the lowest order vertex correction is included in the self-energy and the polarization function. This approach satisfies the Ward–Takahashi identity within the lowest order approximation. As a result, the ionization potential and electron affinity of Li and Li_2 and the optical spectra for sodium clusters are greatly improved compared to the GW and LGW approaches.

Acknowledgements

I would like to express my sincere gratitude to my supervisor, Professor Kaoru Ohno, for supporting and guiding me very kindly.

I also would like to acknowledge Professor Takao Sekiya, Associate professor Ryoen Shirasaki, Associate professor Tetsuji Kuramoto, and Professor emeritus Ken Sasaki for their fruitful comments.

Finally, special thanks to my colleagues in Accelrys K.K. for their encouragement and support.

References

[1] P. Hohenberg and W. Kohn, *Phys. Rev.* **136**, B864–B871 (1964).

[2] W. Kohn, *Rev. Mod. Phys.* **71**, 1253–1266 (1999).

[3] L. Hedin, *Phys. Rev.* **139**, A796–A823 (1965).

[4] G. Baym and L. P. Kadanoff, *Phys. Rev.* **124**, 287–299 (1961).

[5] N. E. Dahlen and R. van Leeuwen, *J. Chem. Phys.* **122**, 164102 (2005).

[6] M. S. Hybertsen and S. G. Louie, *Phys. Rev. B* **34**, 5390–5413 (1986).

[7] E. L. Shirley and R. M. Martin, *Phys. Rev. B* **47**, 15404–15412 (1993).

[8] S. Ishii, K. Ohno, Y. Kawazoe, and S. G. Louie, *Phys. Rev. B* **63**, 155104 (2001).

[9] S. Ishii, K. Ohno, Y. Kawazoe, and S. G. Louie, *Phys. Rev. B* **65**, 245109 (2002).

[10] M. van Schilfgaarde, T. Kotani, and S. Faleev, *Phys. Rev. Lett.* **96**, 226402 (2006).

[11] Y. Takahashi, *Il Nuovo Cimento* **6**, 371–375 (1957).

[12] M. Shishkin, M. Marsman, and G. Kresse, *Phys. Rev. Lett.* **99**, 246403 (2007).

[13] F. Bruneval, F. Sottile, V. Olevano, R. Del Sole, and L. Reining, *Phys. Rev. Lett.* **94**, 186402 (2005).

[14] J. M. Luttinger and J. C. Ward, *Phys. Rev.* **118**, 1417–1427 (1960).

[15] C. Almbladh, U. von Barth, and R. van Leeuwen, *Int. J. Mod. Phys. B* **13**, 535–541 (1999).

[16] F. Aryasetiawan, T. Miyake, and K. Terakura, *Phys. Rev. Lett.* **88**, 166401 (2002).

[17] K. Hongo, R. Maezono, Y. Kawazoe, H. Yasuhara, M. D. Towler, and R. J. Needs, *J. Chem. Phys.* **121**, 7144–7147 (2004).

[18] B. Kovačević, D. Barić, Z. B. Maksić, and T. Müller, *ChemPhysChem* **5**, 1352–1364 (2004).

[19] V. Fock, *Z. Phys.* **63**, 855–858 (1930).

[20] F. W. Averill and G. S. Painter, *Phys. Rev. B* **24**, 6795–6800 (1981).

[21] R. Kuwahara, Y. Tadokoro, and K. Ohno, *J. Chem. Phys.* **141**, 084108 (2014).

[22] R. Kuwahara and K. Ohno, *Mod. Phys. Lett. B* **28**, 1450166 (2014).

[23] A. A. Adllan and A. D. Corso, *J. Phys.: Condens. Matter* **23**, 425501 (2011).

[24] G. E. Engel and B. Farid, *Phys. Rev. B* **47**, 15931–15934 (1993).

[25] W. von der Linden and P. Horsch, *Phys. Rev. B* **37**, 8351–8362 (1988).

[26] S. G. Louie, K.-M. Ho, and M. L. Cohen, *Phys. Rev. B* **19**, 1774–1782 (1979).

[27] W. G. Aulbur, L. Jönsson, and J. W. Wilkins, *Quasiparticle Calculations in Solids*, volume 54 of *Solid State Physics* (Academic Press, 1999).

[28] F. Herman and S. Skillman, *Atomic Structure Calculations* (Prentice Hall, 1963).

[29] J. P. Perdew and A. Zunger, *Phys. Rev. B* **23**, 5048–5079 (1981).

[30] G. Onida, L. Reining, R. W. Godby, R. Del Sole, and W. Andreoni, *Phys. Rev. Lett.* **75**, 818–821 (1995).

[31] B. Delley, *J. Chem. Phys.* **92**, 508–517 (1990).

[32] B. Delley, *J. Chem. Phys.* **113**, 7756–7764 (2000).

[33] C. F. Fischer, *J. Comput. Phys.* **27**, 221 – 240 (1978).

[34] A. Kramida and W. C. Martin, *J. Phys. Chem. Ref. Data* **26**, 1185–1194 (1997).

[35] K. S. E. Eikema, W. Ubachs, W. Vassen, and W. Hogervorst, *Phys. Rev. A* **55**, 1866–1884 (1997).

[36] V. Kaufman and L. Minnhagen, *J. Opt. Soc. Am.* **62**, 92–95 (1972).

[37] V. Kaufman and W. C. Martin, *J. Phys. Chem. Ref. Data* **20**, 83–152 (1991).

[38] I. Velchev, W. Hogervorst, and W. Ubachs, *J. Phys. B* **32**, L511 (1999).

[39] J. Sugar and C. Corliss, *J. Phys. Chem. Ref. Data* **14**, Suppl. 2 (1985).

[40] D. J. Pegg, J. S. Thompson, R. N. Compton, and G. D. Alton, *Phys. Rev. Lett.* **59**, 2267–2270 (1987).

[41] G. Glockler, *Phys. Rev.* **46**, 111–114 (1934).

[42] W. A. Harrison, *Solid State Theory* (Dover, 2011).

[43] R. Kuwahara and K. Ohno, *Phys. Rev. A* **90**, 032506 (2014).

[44] L. Hanley, J. L. Whitten, and S. L. Anderson, *J. Phys. Chem.* **92**, 5803–5812 (1988).

[45] C. J. Reid, *Int. J Mass Spectrom. Ion Proc.* **127**, 147 – 160 (1993).

[46] C. A. Stearns and F. J. Kohl, *J. Phys. Chem.* **77**, 136–138 (1973).

[47] X. Li, H. Wu, X.-B. Wang, and L.-S. Wang, *Phys. Rev. Lett.* **81**, 1909–1912 (1998).

[48] C. B. Winstead, S. J. Paukstis, J. L. Walters, and J. L. Gole, *J. Chem. Phys.* **102**, 1877–1881 (1995).

[49] S. J. Peppernick, K. D. D. Gunaratne, S. G. Sayres, and A. W. Castleman, *J. Chem. Phys.* **132**, 044302 (2010).

[50] N. E. Dahlen, R. van Leeuwen, and U. von Barth, *Phys. Rev. A* **73**, 012511 (2006).

[51] P. Nozières, *Theory Of Interacting Fermi Systems* (Westview Press, 1997).

[52] P. J. Foster, R. E. Leckenby, and E. J. Robbins, *J. Phys. B* **2**, 478 (1969).

[53] D. Feldmann, *Z. Phys. A* **277**, 19–25 (1976).

[54] H. Sarkas, S. Arnold, J. Hendricks, V. Slager, and K. Bowen, *Z. Phys. D* **29**, 209–212 (1994).

[55] A. Herrmann, E. Schumacher, and L. Wöste, *J. Chem. Phys.* **68**, 2327–2336 (1978).

[56] H. Hotop and W. C. Lineberger, *J. Phys. Chem. Ref. Data* **14**, 731–750 (1985).

[57] K. M. McHugh, J. G. Eaton, G. H. Lee, H. W. Sarkas, L. H. Kidder, J. T. Snodgrass, M. R. Manaa, and K. H. Bowen, *J. Chem. Phys.* **91**, 3792–3793 (1989).

[58] K. Huber and G. Herzberg, *Molecular Spectra And Molecular Structure. IV. Constants Of Diatomic Molecules* (Van Nostrand, 1979).